CrossMark

The regional impact of Land-Use Land-cover Change (LULCC) over West Africa from an ensemble of global climate models under the auspices of the WAMME2 project

Aaron Anthony Boone[1] · Yongkang Xue[2] · Fernando De Sales[7] · Ruth E. Comer[4] ·
Samson Hagos[5] · Sarith Mahanama[6] · Kathleen Schiro[2] · Guoqiong Song[2] ·
Guiling Wang[3] · S. Li[2] · Carlos R. Mechoso[2]

Abstract The population of the Sahel region of West Africa has approximately doubled in the past 50 years, and could potentially double again by the middle of this century. This has led to the northward expansion of agricultural areas at the expense of natural savanna, leading to widespread land use -land cover change (LULCC). Because there is strong evidence of significant surface-atmosphere coupling in this region, one of the main goals of the West African Monsoon Modeling and Evaluation project phase II is to provide basic understanding of LULCC on the regional climate, and to evaluate the sensitivity of the seasonal variability of the West African Monsoon to LULCC. The prescribed LULCC is based on the changes from 1950 through 1990, representing a maximum feasible degradation scenario in the past half century. It is applied to 5 state of the art global climate models (GCMs) over a 6-year simulation period. Multiple GCMs are used because the magnitude of the impact of LULCC depends on model-dependent coupling strength between the surface and the overlying atmosphere, the magnitude of the surface biophysical changes, and how the key processes linking the surface with the atmosphere are parameterized within a particular model framework. Land cover maps and surface parameters may vary widely among models; therefore a special effort was made to impose consistent biogeophysical responses of surface parameters to LULCC using a simple experimental setup. The prescribed LULCC corresponds to degraded vegetation conditions, which mainly cause increases in the Bowen ratio and decreases in the surface net radiation, and result in a significant reduction in surface evaporation (upwards of 1 mm day^{-1} over a large part of the Sahel). This, in turn, mainly leads to less moisture convergence and precipitation over the LULCC zone. The overall impact is a rainfall reduction with every model, which ranges across models from 4 to 25 % averaged over the Sahel, and a southward shift of the rainfall peak in three of the five models which evokes a precipitation dipole pattern which is consistent with the observed pattern for dry climate anomalies over this region. The African Easterly Jet shifts equator-ward, although the strength of this change varies considerably among the models. In most of the models, the main factor causing diabatic cooling of the upper troposphere and enhanced subsidence over the region of LULCC is the reduction of convective heating rates linked to reduced latent heat flux and moisture flux convergence. In broad agreement with previous studies, the impact of degradation on the regional climate is found to vary among the different models, however, the signal is stronger and more consistent between the models here than in previous inter-comparison projects. This is likely related to our

✉ Aaron Anthony Boone
aaron.a.boone@gmail.com

[1] CNRM UMR 3589, Météo-France/CNRS, Toulouse, France

[2] University of California, Los Angeles, CA, USA

[3] University of Connecticut, Storrs, CT, USA

[4] Met Office Hadley Centre, Exeter, UK

[5] Pacific Northwest National Laboratory, Richland, WA, USA

[6] SSAI, Lanham, MD, and Global Modeling and Assimilation Office, NASA Goddard Space Flight Center, Greenbelt, MD, USA

[7] San Diego State University, San Diego, CA, USA

emphasis on prioritizing a consistent impact of LULCC on the surface biophysical properties.

1 Introduction

The population of the Sahel region of West Africa has approximately doubled in the past 50 years, and could potentially double again by the middle of this century. This increase will put ever more pressure on the already limited water and agricultural resources in the region. In recent years, food production has indeed increased, but this has been mostly due to increases in the surface area cultivated (230 %) rather than actual yield (42 %) (Blein et al. 2008). This increase has led to the expansion of agricultural and pasture areas at the expense of natural savanna and forests (e.g. Leblanc et al. 2008), leading to widespread land use and land cover change (LULCC). These changes can lead to land degradation, and some of the most general causes are overgrazing, continuous cropping, deforestation for firewood, and mismanagement of soil and water resources.

The land surface has been shown to be an important factor in modulating the West African monsoon (WAM). For example, based on observations, the land surface characteristics and processes have been shown to have a significant impact on the inter-annual variability of rainfall in the Sahel region (Nicholson 2013). The importance of surface-atmosphere interactions was one of the main tenets of the recent international African Monsoon Multidisciplinary Analysis (AMMA) project (Redelsperger et al. 2006) and was investigated in several studies (see Taylor et al. 2011, for a summary). This region typically appears as one where the soil moisture feedbacks with the atmosphere are among the strongest over the globe (e.g. Dirmeyer 2011). Using an ensemble of state-of-the-art global climate models (GCMs), the Sahel region has been identified as one of strong soil moisture-atmosphere coupling (Koster et al. 2004). In addition, it has been determined to be the region of the world with the highest impact of biophysical processes on the climate (Xue et al. 2004, 2010b). Indeed many numerical studies have shown the importance of the land surface on modulating the WAM (for a review, see Xue et al. 2012). For example, previous studies have examined the role of changes in the surface albedo (e.g. Charney 1975; Sud and Fennessy 1982; Laval and Picon 1986) and the vegetation (e.g. Xue et al. 1990; Xue 1997; Zheng and Eltahir 1997; Li et al. 2007) on modulating the WAM. All of these studies lead to the general conclusion that reduced vegetation leads to reduced rainfall. Most of these studies

were based on sensitivity experiments using single GCMs and land surface models (LSMs), which have model-specific LULC classifications, with idealized and sometimes extreme LULCC scenarios.

There is increasing evidence from numerical studies that anthropogenic LULCC can potentially induce significant variations on the local to regional scale climate (Pielke et al. 2011). However, the IPCC's Fifth Assessment lacked a comprehensive evaluation of the relative impact of biogeophysical feedbacks of LULCC on regional climate (Mahmood et al. 2014). This is primarily due to oversimplifications and limits to how some key biogeophysical surface processes are represented in the LSM component of GCMs, and how LULC is represented in such models. The recent Land-Use and Climate Identification of robust impacts (LUCID) experiment (Pitman et al. 2009; de Noblet-Ducoudré et al. 2012) examined the biogeophysical impacts of prescribed, global-scale LULCC using an ensemble of coupled GCMs and LSMs. The goal was to identify impacts that were statistically robust, primarily in terms of being detectable, common among the different models, and above the models' internal variability. LULCC was prescribed based on historical data, with changes based on the time period starting with the beginning of the industrial revolution to present day conditions. LSM models modified their land cover (following their own classification) on the non-crop areas in order to adhere to these changes as much as possible. There turned out to be considerable discrepancy among the models in terms of their response to LULCC, particularly in terms of the Bowen ratio. In addition, LULCC-induced changes in surface sensible heat and latent heat fluxes had opposite signs in some regions among the different models. Reasons for discrepancies are likely related to differences in the land surface parameterizations: for example, how soil moisture is taken up by transpiration, the treatment of turbulence in the surface layer, vadose-zone hydrology and surface runoff production, and the use of dynamic verses prescribed vegetation. The definition of land use classes can also be a source of significant differences. For example, a crop class in one model might be represented as natural grasses in another model: not only can this result in important differences in the values of certain key biogeophysical parameters, it can also cause differences in terms of the imposed seasonal evolution of these parameters. In addition, two models might use the same class for a given vegetation cover, but very different values of the same parameters that characterize the vegetation (such as structural parameters). Different modeling groups have developed special methodologies for changing land cover distributions, which can lead to discrepancies. Another obvious source of differences results from inter-model variations of the simulated coupling strength between the surface and the atmosphere (Koster

et al. 2004). In addition to being related to the LSM physics, the coupling strength is also influenced by the physical parameterizations in the different host atmospheric models, notably the parameterizations of planetary boundary layer (PBL, turbulence), convection, clouds, and atmospheric radiation.

One of the main goals of the West African Monsoon Modeling and Evaluation project phase II (WAMMEII) is to provide a basic understanding of LULCC forcing on the regional climate of West Africa (Xue et al. 2016, this issue). The strategy is to apply observational data-based anomaly forcing, i.e., "idealized but realistic", in GCM and RCM simulations. The prescribed LULCC is based on data from Hurtt et al. (2006) which was used to design a maximum feasible degradation scenario, which will be discussed in Sect. 2.1. In the current study, 5 state-of-the-art GCMs are used in order to study a range of model responses to a common LULCC scenario with a focus on West Africa. In addition, two GCMs use the same LSM (so presumably differences only arise owing to atmospheric effects between these two models), and two models performed two simulations with varying degrees of LULCC. The model intercomparison results for RCMs are reported by Hagos et al. (2014) and Wang et al. (2015). This paper is organized as follows: the methodology for imposing LULCC for multiple GCMs is summarized in Sect. 2, results are presented in Sect. 3, a summary of the main impacts of LULCC on the WAM are summarized in Sect. 4, along with the conclusions of this study.

2 Experimental design

2.1 LULCC methodology

The definition of a control vegetation map is a complicated issue owing to many factors. Due to the errors in satellite data acquisition, data processing, information extraction methodologies, inadequate ancillary training data, as well as the relatively course resolution in current climate models, current satellite-derived vegetation maps have difficulties with respect to adequately present realistic LULC information. This is especially true over West Africa, where the agricultural areas are generally poorly classified. These potential vegetation maps are often based upon remote sensing-produced vegetation maps. This is the current status of terrestrial remote sensing (e.g. Kim et al. 2015), and the experimental design has to take this into account. Thus, in the current study, LULCC is applied to the default current map for each model (which for many models consists in either constant class-based vegetation indices or some sort of climatological annual cycle). The LULCC experiment uses combined crop and pasture fraction changes

from Hurtt et al. (2006). This data set was used by the 5th Assessment Report (AR5) of the Intergovernmental Panel on Climate Change (IPCC 2014) and was used in the Coupled Model Intercomparison Project (CMIP5) project (Taylor et al. 2012a, b). Note that the dataset used in this study is based on land use change that occurred from 1950 to 1990 which showed a dramatic land degradation in West Africa and became less pronounced (more flat) afterwards (Song 2013). The data has been translated into LULCC for each of the models participating in the present study. Note that the actual changes in land use are not conserved when transformed into model parameter space because each model has their own implementation strategy. Thus, the total LULCC is meant to represent the maximum feasible total amount of degradation resulting from anthropization (i.e. the conversion of natural vegetation, mainly savanna and low trees or shrubs, to cropland or pasture). This is an important distinction from some of the studies mentioned in the previous section (Pitman et al. 2009; de Noblet-Ducoudré et al. 2012), which can potentially include regions where vegetation has returned to a so-called natural state. In addition, another important distinction is that this study prioritizes degradation that is consistent in terms of the biogeophysical response of the surface, as opposed to a consistent land classification change. This is done because two models can impose similar LULCC but produce very different results in terms of the biophysical response, i.e. the values of surface physiographic parameters.

The land cover is only changed over West Africa within the Sahel and over an area extending southward of the Sahel which mainly covers the extreme eastern portions of Guinea and Liberia, Ivory Coast and Ghana. Note that there can be some ambiguity when applying such definitions to West Africa: distinguishing between pasture and cropland can be difficult in this region since animals will oftentimes graze in crop fields after harvest (P. Hiernaux, personal communication). This data set, however, represents the current state-of-the-art on the global and therefore it is used as guideline to provide a maximum reasonable LULCC scenario. A simple methodology has been developed using the following criteria:

1. Making consistent LULCC in vegetation maps among models. Also, since significant differences are caused by different map spatial resolutions, a specified LULCC region that is broad enough to be used by even the most coarse resolution models (and has a relatively simple geometrical configuration) was defined. The maximum land class change permitted within a particular grid cell was constrained to be less than or equal to the maximum change estimated from the historical land use data set used in this study over the Sahel for the specified time period.

Table 1 A summary of the WAMME2 models performing the LULCC experiments

GCM (acronym used in Figs.)	Contact	Resolution	Convection	Radiation	LULC (number of classes)	Land surface model
UCLA-AGCM (UCLA-AGCM) Mechoso et al. (2000)	C. R. Mechoso K. Schiro	$2.5° \times 2° \times L17$	Prognostic version of Arakawa and Schubert (1974)	Harshvardhan et al. (1987)	Dominant (12)	SSIB-1 Xue et al. (1991)
UCLA-GFS (UCLA-GSM) Kanamitsu et al. (2002), Xue et al. (2004)	Y. Xue, F. De Sales	T62L28	Moorthi and Suarez (1992)	Chou and Suarez (1994)	Dominant (12)	SSIB-1 Xue et al. (1991)
UCONN CAM5 (CAM5)	G. Wang	T63L26	Zhang and McFarlane (1995)	Iacono et al. (2008)	Tiles (17)	CLM Oleson et al. (2008)
GSFC GOES-5 (GMAO)	S., Mahanama, R. Koster	$1° \times 1.25° \times L72$	Moorthi and Suarez (1992)	Chou et al. (2001)	Tiles (6)	CLSM Koster et al. (2000)
UKMO HadGEM 2-A (HadGEM) HadGEM2 model development team (2011)	R. Comer	$1.25° \times 1.875° \times L38$	Derbyshire (2011)	Edwards and Slingo (1996)	Tiles (9)	MOSES Essery et al. (2002)

The model acronyms used in the text are enclosed by parentheses in the leftmost column

2. Proposing the modifications to the land class in the grid points associated with LULCC based on historical land use change information, and determining a set of corresponding surface parameters after careful coordination with each of the different modeling groups.

3. Maintaining a consistent meridional gradient of the LULCC in terms of the surface vegetation distribution, in an attempt to ensure that the prescribed changes to the surface parameters truly correspond to a consistent degradation in the land maps among the models.

2.2 LULCC implementation

Five GCMs participated in this experiment, and they are listed along with their corresponding LSM in Table 1. Two distinct GCMs used at the University of California at Los Angeles (UCLA) contributed simulations to this study: the UCLA AGCM and the UCLA GFS (referred to hereafter as UCLA-GSM). HadGEM2 represents the Hadley Centre Global Environmental Model, version 2. The GEOS-5 (the version 5 of the Goddard Earth Observing System Model) of the Global Modeling and Assimilation Office at NASA/GSFC is referred to as GMAO in this paper. CAM5 refers to the National Center for Atmospheric Research (NCAR) Community Atmospheric Model version 5. See Table 1 for a complete set of references for all of the models used in this study. In the control (CTL) experiment, the native "climatological" vegetation map (or set of biogeophysical parameters) is used by the model groups. The only
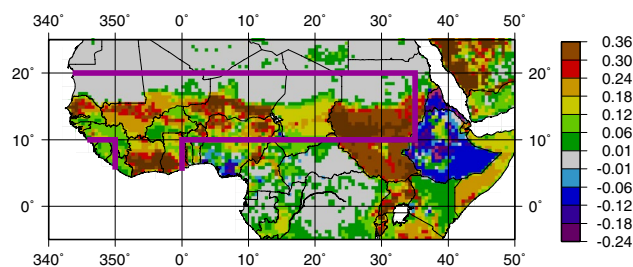

Fig. 1 The LULCC is applied within the zone bounded by the *purple lines*. The *color scale* corresponds to the fractional change in the combined crop and pasture fractions. This region includes the Sahel, but also Ivory Coast and Ghana (south of 10° N) owing to the significant LULCC in that region

difference between the forcing used in the LULCC experiment, here to after referred to as Exp. LULCC, and Exp. CTL results from changes to the land cover. The LULCC is defined as the difference in total crop and pasture fraction between 1990 and 1950, and it is shown in Fig. 1. Since our focus is on the Sahel, the LULCC is only imposed within the bounded region enclosed by purple lines. This region encompasses the Sahel, where population and pressure on limited water resources are expected to increase the most over the upcoming decades. Another region covering the Ivory Coast and Ghana is also included because the land use change is marked in this region. The mask is relatively simple geometrically in order to accommodate the varying model grid resolutions and to facilitate both the implementation in the models and analysis of the impacts. In
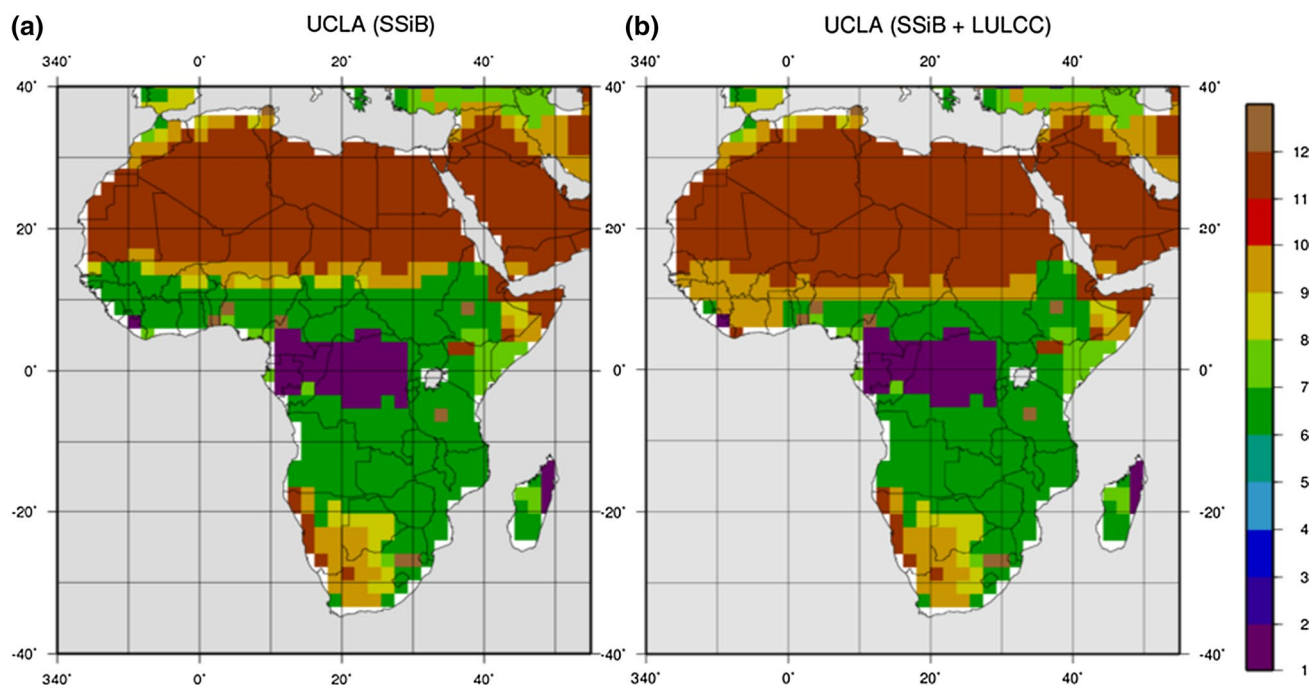
Fig. 2 An example of LULCC for the UCLA models (which use the SSiB land surface model). The default land class data are shown in panel (**a**). In panel (**b**), we have changed classes 6–9 (broadleaf trees with ground cover to broadleaf shrubs with baresoil), 7–11 (ground cover to baresoil) and 9–11 (broadleaf shrubs and baresoil to baresoil) over the masked zone

addition, climatological sea surface temperatures (SST) are used. Each experiment runs for 6 years starting on January 1, 2006, but the first year is regarded as spin-up and is therefore removed from the analysis.

The basic LULCC map was first provided to participants. The land cover fraction change is limited to 30 % in the current study. This threshold was selected in order to avoid any isolated grid points with had anomalously high LULCC that could produce small scale noise in the GCM response since, as seen in Fig. 1, only a few relatively small areas have changes larger than this threshold. This limit was imposed also under the consideration of the selection criteria number 3. After testing the LULCC within the different vegetation maps used by the models, this criteria seems to serve the best to produce a reasonable gradient. The next step was to compare the control and modified *LAI* and albedo fields across the modeling groups to ensure that the land class changes result in surface changes that are as consistent as possible among the different models. If a change was found to be inconsistent with the other models or not representative of a degradation, further modifications were made to the land cover in order to obtain a similar biogeophysical response. Potentially several iterations with each participating group were used to achieve this goal.

There are essentially two different strategies for defining surface parameters as a function of land use in the models used in the present study. The UCLA-AGCM and UCLA-GSM use the Simplified Simple Biosphere (SSiB; Xue et al. 1991) LSM and the corresponding land use classification map (look-up table) for assigning surface properties (the dominant class for each grid box). These models used the standard SSiB vegetation map (12 types) which is based on AVHRR data and is fixed over time (Hansen et al. 2000). The LAI and vegetation albedo climatological annual cycles are prescribed for each vegetation class. Soil albedo is also fixed over time for the current study. The LULCC consisted in replacing a fraction of (1) broadleaf trees with ground cover to broadleaf shrubs with baresoil, (2) low vegetation-ground cover to baresoil, and (3) broadleaf shrubs and baresoil to baresoil. An example of the impact of LULCC is shown in Fig. 2. Essentially, forests become grassland/crop regions, and savanna or semi-arid transition zones become mainly bare soil regions. This represents the most simple LULCC implementation. Upon examination of this and the other WAMME GCMs' vegetation maps (not shown), it becomes apparent that they are no more than general potential vegetation maps. Thus, it is hard to draw LULCC information from them when compared with the vegetation maps in the 1980s, such as that of Kuchler (1983).

The second LSM strategy can represent multiple LULC within the same grid box using specific sub-grid tile fractions. The HadGEM Met Office Surface Exchange Scheme (MOSES; Essery et al. 2002) uses the International

Geosphere–Biosphere Programme (IGBP) global land cover classification (IGBP 1992) with 9 classes. The back ground soil/litter albedo varies in space (Houldcroft et al. 2009) and is independent of land cover class. The vegetation albedo is fixed for each of the 9 classes, and has no temporal variation. The initial LAI values at the start of the 6-year integration period are derived from MODIS satellite products. The MOSES vegetation phenology module was activated, thus the LAI varies in time for each of the tiles (classes present in this zone). The impact of the LULCC on the land cover can be summarized as follows: broadleaf trees decreased by upwards of 30 %, and grasses decrease by approximately half that value, where the existing ratio of C3–C4 grasses was held constant for each grid cell. Shrub lands decrease in the northern Sahel, but increase to the south (mostly in place of decreased forest). The baresoil fraction increases upwards of 30 %. Two LULCC scenarios are analyzed in the current study. For the default LULCC study, the background soil/litter albedo was increased (to be more like values further north: the values were adjusted so that the Sahel average equals 0.35). This resulted in local changes as high as 0.15, but the average increase over the LULCC zone is approximately half of that value). In the sensitivity test (HadGEM-w: see Sect. 3.4), the background albedo was unchanged.

The CAM5 surface scheme (Common Land Model or CLM; Oleson et al. 2008) can represent up to 17 subgrid tiles within each grid cell (with 16 being plant functional types or PFTs). It was developed for CLM by Lawrence and Chase (2007) and it uses MODIS-based data for trees, and IGBP data for shrubs and grasses, and data from Ramankutty et al. (2008) for crops. For the current study, LAI varies on a daily basis based on linear interpolation of monthly varying LAI, and the annual cycle is fixed for all 6 years. The soil albedo dynamic range (for moisture saturated and totally dry conditions) is specified, and it varies in time as a function of soil moisture. The soil albedo at saturation is entirely determined by soil color which is an independent spatially varying field. The LULCC consisted in changing the forest (PFTs 5 and 7) to grass (PFT 15), and shrub (PFT 11) to baresoil (PFT 1) within the masked zone. The sum of deforestation and desertification areas was limited locally to 30 %. The soil color was modified to obtain albedo changes similar to the other models.

The GMAO surface scheme (Catchment Land Surface Model, CLSM: Koster et al. 2000) uses 6 tiles. The LAI and Greenness fraction (Grn) monthly climatologies are from global satellite observations along with a model-based surface albedo which has been scaled to match the mean seasonal cycle of MODIS satellite observations. Compared to the other GCMs, the GMAO uses a different methodology for assigning parameter values. A vegetation map that evolves in time during the integration (the CTL LULC is

from 1952 to 1957) is used. Within the LULCC domain, LAI and albedo vary inter-annually as a result of the time varying tile fractions, while outside of the domain a fixed annual cycle was used. The LULCC for the sensitivity test (GMAO-w; see Sect. 3.4) used the GMAO default long-term integration setup for which only the tile fractions are varied based on data from Hurtt et al. (2006). As it turns out, the sensitivity of surface fluxes to vegetation classes is significantly smaller than that of the prescribed LAI, Grn, and albedo data. Thus, the default LULCC experiment in the current study (referred to as GMAO) required the development of a parameter data set to mimic land use change/degradation over a period of 50 years. In the LULCC experiment, the LAI was approximately halved and the albedo was approximately doubled compared to GMAO-w. This underscores the difficulty in developing a consistent LULCC, especially in terms of the vegetation structural parameters and coverage.

2.3 Experimental protocol

The CTL experiment protocol is described in detail in Xue et al. (2016: this issue), so only a brief summary is provided herein. GCM models are initialized on January 1, 2006, and then run for 6 years. Time varying sea surface temperatures from correspond to a single climatological annual cycle. The first year results are discarded to minimize the potential impact of model spin up. Since the main forcings are the same for all 6 years, the remaining simulations are treated as a 5-member ensemble for each model when doing the results analysis. The atmospheric initial conditions are from the NCEP/DOE (National Center for Environmental Prediction–Department of Energy) Reanalysis II (Kanamitsu et al. 2002). The LULCC experiment uses the same initial conditions and SST forcings, the only difference is in the land cover parameters within the LULCC zone over West Africa.

3 Results

In this section, "differences" are computed by subtracting mean variables obtained in Exp. CTL from those obtained in Exp. LULCC. The impact of LULCC was found to be largest mainly during the peak monsoon months (here meaning peak Sahelian climatological rainfall, i.e. JAS: July, August, September). In the CTL and LULCC experiments, 61 and 63 %, respectively, of the annual rainfall within the Sahel and Ghana regions (LULCC area shown in Fig. 1) averaged for the 5 GCMs fell during this 3 month period. Therefore, the analysis presented in this study focuses on JAS averages. Note that since the prescribed SSTs are climatological, the last 5 years of the six-year

simulations are used as a 5-member ensemble for each of the GCMs and for the multi-model ensemble for computing statistics. A two-tailed student t test is used to test for significance of the local mean values at the 5 and 10 % confidence levels. The significance levels are computed using the pool permutation procedure (PPP), which has been used to inter-compare global multi-model results (e.g. Santer and Wigley 1990). This method accounts for the effects of multiplicity and spatial autocorrelation, and provides estimates of field significance level (p value) for a given number of permutations: 1000 were used to compute statistics in the current study. The impact of LULCC is mainly confined to the region referred to herein as the analysis domain where surface properties were modified, therefore the aforementioned statistics were computed over the domain from 5° to 20° North latitude, and −10°–30° East longitude.

3.1 Impact of LULCC on surface properties

The following analysis focuses on two key land surface parameters that have similar meanings among the LSMs and can be estimated from satellite data: (1) the surface albedo, and (2) the *LAI*. The albedo controls the total enthalpy flux exchange with the atmosphere (a larger albedo implies less energy available for surface turbulent fluxes of heat and/or moisture) and is therefore linked to moist convection, while the *LAI* modulates the Bowen ratio (defined as the ratio of sensible to latent heat flux) for regions where the vegetation coverage is significant. The CTL *LAI* averaged for July–August (JAS) during 5-year simulation is shown in Fig. 3 (left column) for the 4 different models (the two UCLA GCMs have the same land map and land data set). Several features can be highlighted. The UCLA GCMs have the largest average *LAI* values (approximately 4.1 $m^2\ m^{-2}$) in the LULCC region, by nearly a factor of 2, on average, compared to the other models. The remaining models, which use the tile approach, have generally lower values and a smoother meridional gradient across the Sahel. The CAM5 and GMAO models have very similar *LAI* values and spatial distributions, except just south of 10° N. In this region, GMAO has relatively low *LAI* values corresponding to sparse grass. Finally, the HadGEM *LAI* has nearly the same spatial distribution as for the CAM5 GCM, but with values that are approximately 50 % higher. This highlights how both the values and spatial distributions of observable biogeophysical parameters can vary among the models. The impact of the LULCC on the *LAI* is shown in Fig. 3 (right column). The models using the single dominant vegetation type per grid box (UCLA) have a significant relative change in *LAI* (slightly over 3 $m^2\ m^{-2}$) along the southern Sahel, Ivory Coast and Ghana. Despite the fact that the HadGEM has a larger *LAI* than GMAO, the LULCC is quite similar in magnitude and spatial distribution. The CAM5 changes are the weakest in terms of magnitude. This is significant since changes in this parameter generally can have a particularly large impact on the Bowen ratio in water-limited regions (Pielke et al. 2011).

The difference between the JAS average in the Exp. CTL and Exp. LULCC total effective surface albedo is shown in Fig. 4. This parameter is defined as the ratio of the total reflected shortwave radiation to the downwelling flux at the surface. In all cases, the albedo increases in response to degradation. However, the degree of change varies significantly among the models. In terms of the default LULCC, the HadGEM (Fig. 4f) has the largest changes (locally upwards of 0.15, although the regional scale average is approximately half this value). Peak changes in the UCLA models are also significant (Fig. 4a, b), with values of 0.09 (the domain-average change is larger in UCLA-GSM). The CAM5 (Fig. 4g) model has slightly lower changes (upwards of 0.06), but some areas with very small changes are interspersed. Note that by simply imposing the prescribed land class changes, the albedo increased by approximately 3 times less than the values shown in Fig. 4g, thus the soil color was also modified in order to obtain the changes used in this study. This underscores once again the subtleties required to obtain a consistent response in terms of biogeophysical properties to LULCC among models. The GMAO model has peak albedo changes in the northernmost, driest portion of the Sahel, in contrast to the other models. This feature turns out to be significant in terms of the LULCC impact (as discussed in subsequent sections). Finally, both GMAO and CAM5 show little change in albedo over the Ivory Coast-Ghana regions, in contrast with relatively significant *LAI* decreases. It should be pointed out that in the early study by Charney et al. (1977), a dramatic albedo change (0.21 over the entire longitudinal band centered over the Sahel) was prescribed in order to obtain a significant response. This specification has been used as evidence to discredit the potential role of LULCC in terms of Sahel drought. Later observation-based studies (e.g. Nicholson et al. 1998; Govaerts and Lattanzio 2008) have suggested that albedo changes over the Sahel of around 0.1 (with locally higher values upwards of 0.15 in the latter study) over the period of several decades are possible. In these studies, the albedo increases were found to be mainly related to differences between relatively wet and dry years. Currently, we can distinguish whether these changes were due to natural or anthropogenic causes, and/or both. In terms of total area impacted by LULCC, notable changes to *LAI* and albedo extend to the southern limit of the desert (Figs. 3, 4, respectively) there by covering most of the

Fig. 3 The CTL JAS-average leaf area index (*LAI*: $m^2 \, m^{-2}$) for each of the GCMs are shown in the *left column*. The difference between the LULCC and the CTL values are shown in the *right column*. Note that the two UCLA models (GSM and AGCM) use the same LSM and land cover (*panels* **a**, **b**)
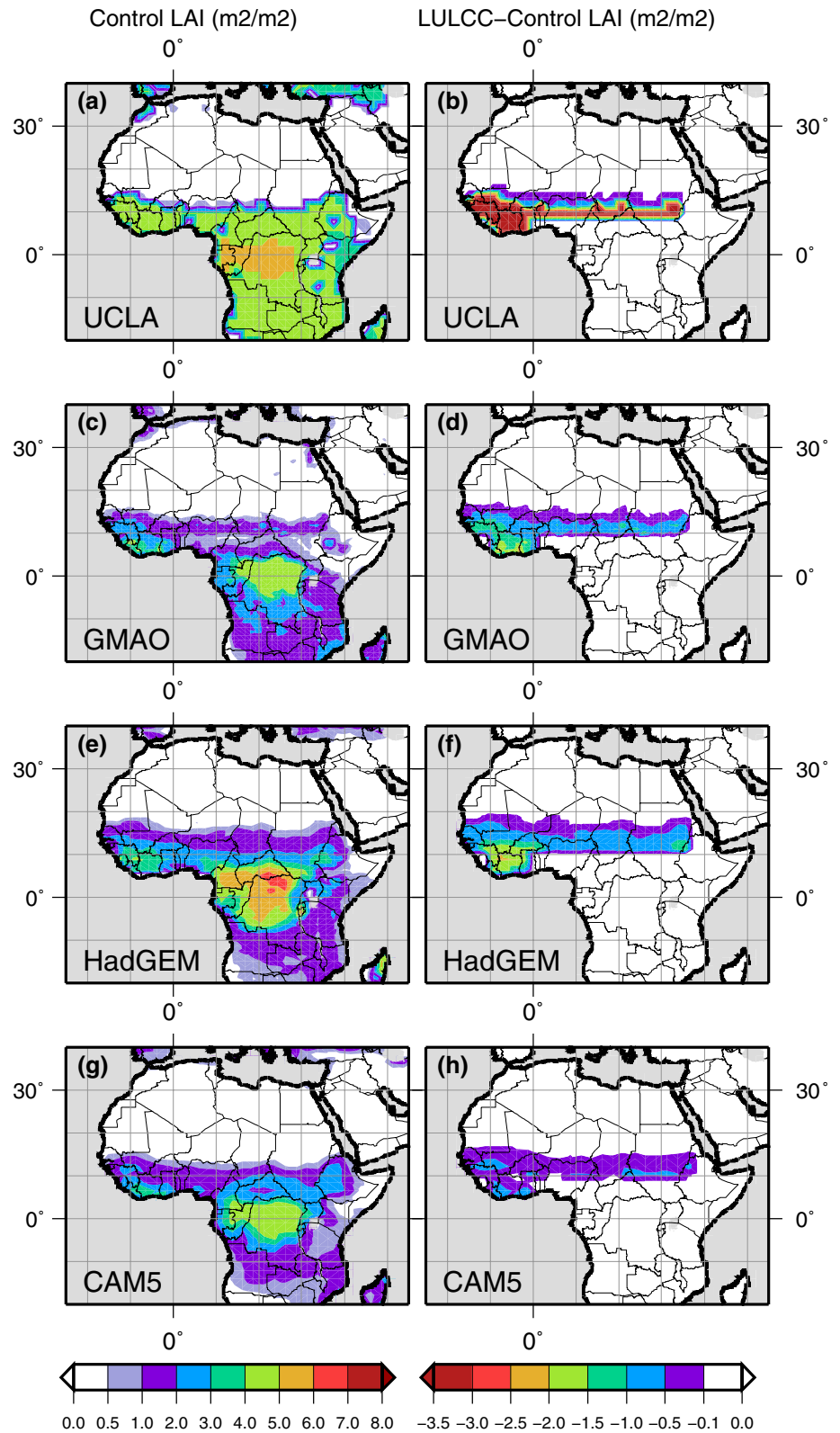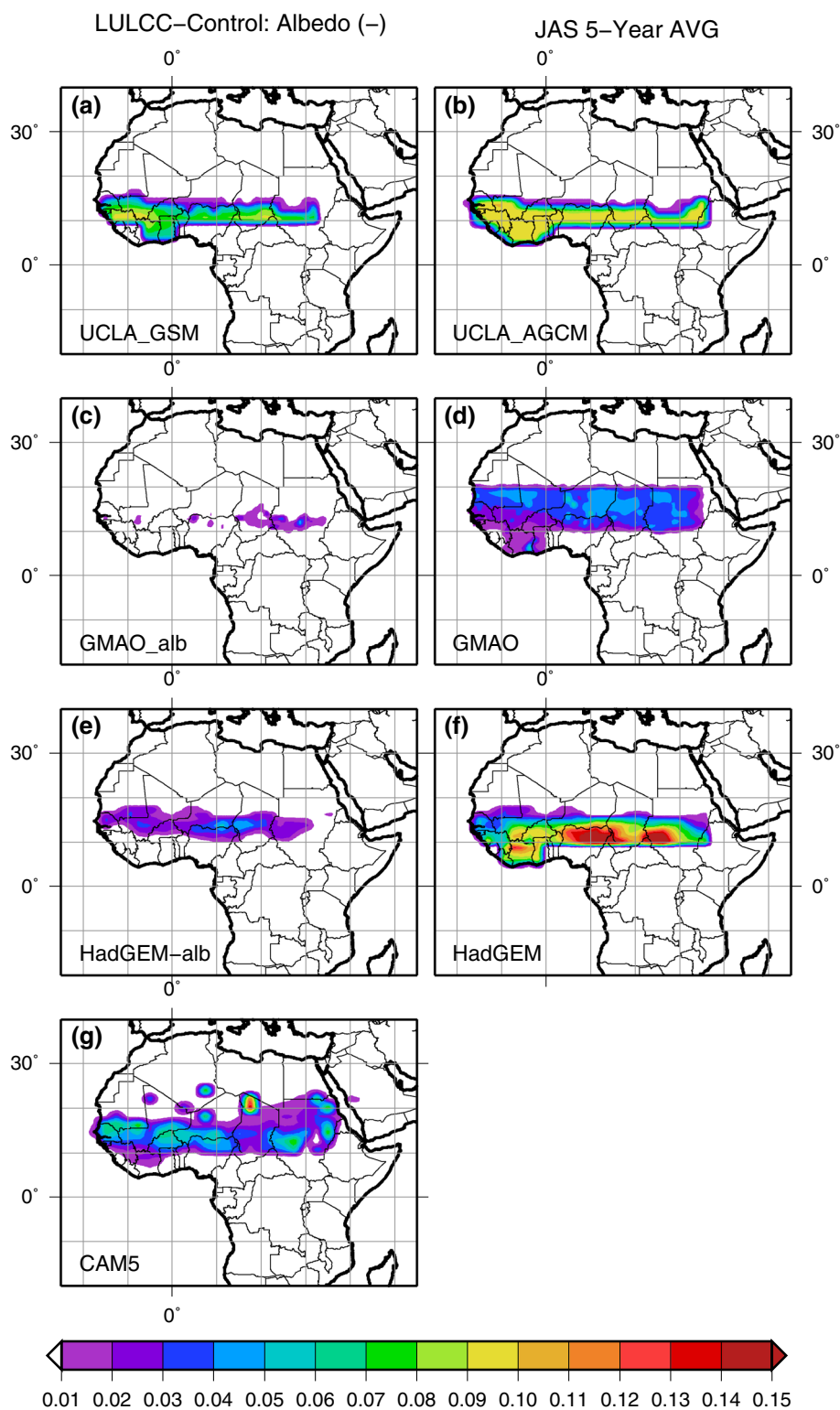
Fig. 4 The change in effective surface JAS albedo (the LULCC less the CTL values). Note that panels **c** and **e** correspond to sensitivity tests (see Sect. 3.4)


LULCC zone shown in Fig. 1 for four of the models (the two UCLA models, HadGEM and CAM5). The total area impacted for the GMAO model cover the entire region of imposed LULCC (Fig. 1) since albedo changes also occur in the desert region (Fig. 4f).

3.2 Impact of LULCC on surface fluxes

The first order impact of the change in land cover is on the surface fluxes. The results for the surface fluxes are only presented over West Africa, since there was virtually

**Fig. 5** The JAS average *LE* (surface latent heat flux: W m^{-2})
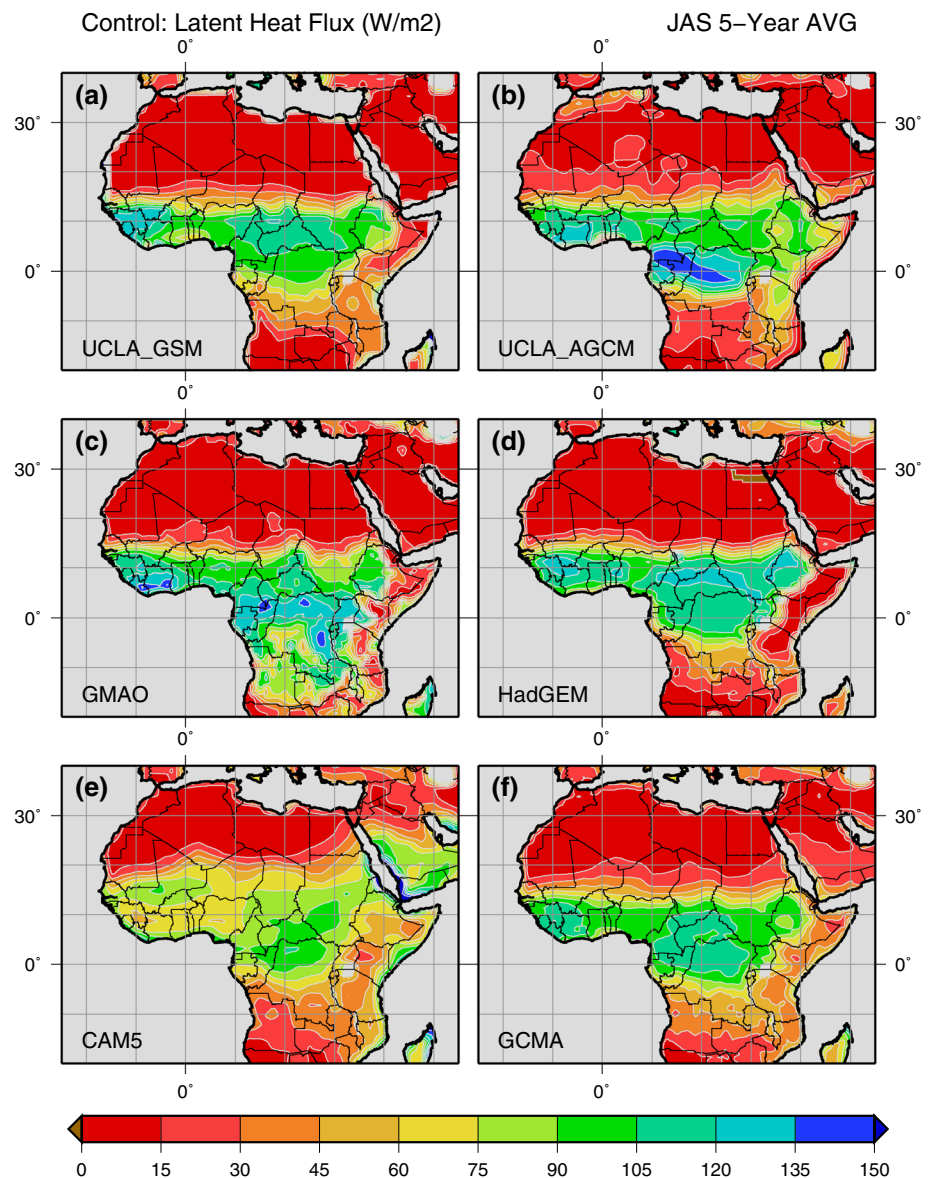
no appreciable effect on surface fluxes nor statistical significance above 95 % for a two-tailed t-test outside of this region (the relatively local nature of the impact of LULCC on the surface fluxes is consistent with the findings of Pitman et al. 2009; de Noblet-Ducoudré et al. 2012). The JAS average latent heat flux, *LE*, is shown for each GCM, along with the five-model average (GCMA) in Fig. 5. Four of the five models simulate a significant *LE* meridional gradient, in relation to the rainfall, in the Sahel (between 10° and 20° N). The CAM5 model simulates *LE* and rainfall further north than the other models, along with the lowest latent fluxes over the entire region. In contrast, the GMAO model simulates peak *LE* over West Africa along the southern coast. The UCLA models show a distinct minimum of *LE* near southern Ghana, Togo and Benin, so that the main rainfall band is further inland. The HadGEM is an

intermediate case (peak rainfall between the UCLA and GMAO models). The position of the WAM and its intensity (characterized by the rainfall) varies considerably among GCM models (examples from recent inter-comparison projects: Hourdin et al. 2010; Roehrig et al. 2013).

The JAS average change in surface net radiation, *Rnet*, latent heat flux, *LE*, and sensible heat flux, *H*, are shown in Figs. 6, 7, 8, respectively. The green contour line encloses regions where the differences are significant at the 95 % confidence level for a two-tailed student *t* test. A statistical summary is shown in Table 4. The percentage of the analysis domain for which are significant above the 90 and 95 % confidence levels using a two-tailed student *t* test are referred to as NT10 and NT05, respectively. The corresponding p-values from the PPP test (given in parenthesis) indicate the significance level. The signature of the

Fig. 6 The JAS average difference in surface net radiation, *Rnet* (LULCC less the CTL values; W m^{-2}). Contours correspond to the 95 % confidence level
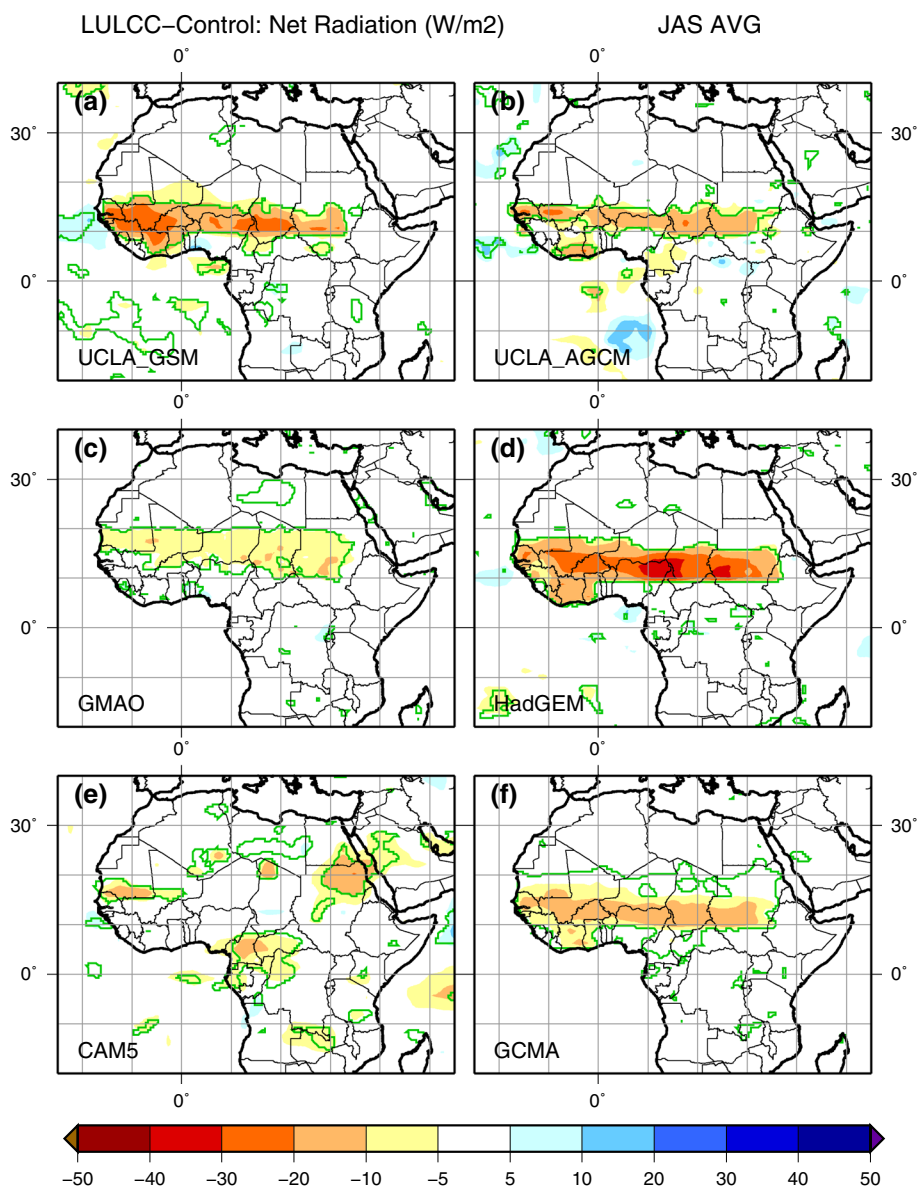
albedo change in terms of *Rnet* (Fig. 6) is clearly seen in four of the five models. The exception is CAM5, for which *Rnet* is only impacted in a small zone over the extreme west and another over western Sudan. This means that for this model, other factors controlling the *Rnet* (such as changes in the upwelling surface longwave radiation and downwelling fluxes) are compensating the albedo changes over most of the Sahel. The multi-model average, GCMA, changes are shown in Fig. 7f, and the signal is fairly robust over (and slightly outside of) the entire LULCC region (Fig. 1). The changes in *LE* are shown in Fig. 7. The HadGEM *LE* decreases result almost entirely from the *Rnet* reductions. Comparison with the CTL *LE* (Fig. 5) reveals that the relative reduction generally ranges from approximately 10–30 % over the Sahel. For both UCLA models, the *LE* decreases are equal to or even exceed the

Rnet decreases (in the extreme western Sahel for UCLA-GSM, with *LE* reductions upwards of 50 %, and over the Ivory Coast region for the UCLA-AGCM, with *LE* reductions there on the order of 30 %). Owing to surface energy budget conservation, these two models have increases in the sensible heat flux, *H*, over the aforementioned regions (see Fig. 8a, b) that are related to significant changes in the Bowen ratio (resulting mainly from significant reductions in *LAI*, see Fig. 4a, b). The *Rnet* signature is weak in the GMAO *LE*, since the albedo changes occurred mostly north of the area receiving precipitation. The only areas with notable *LE* decreases are over the extreme western Sahel and southern Ivory-coast and Ghana regions, associated with reduced *LAI*. The CAM5 *LE* is reduced along the southern Sahara: this turns out to be related to a significant southward shift in the WAM for this model (more details

Fig. 7 As in Fig. 6, except for latent heat flux, *LE* (W m^{-2})

LULCC–Control: Latent Heat Flux (W/m2)   JAS AVG
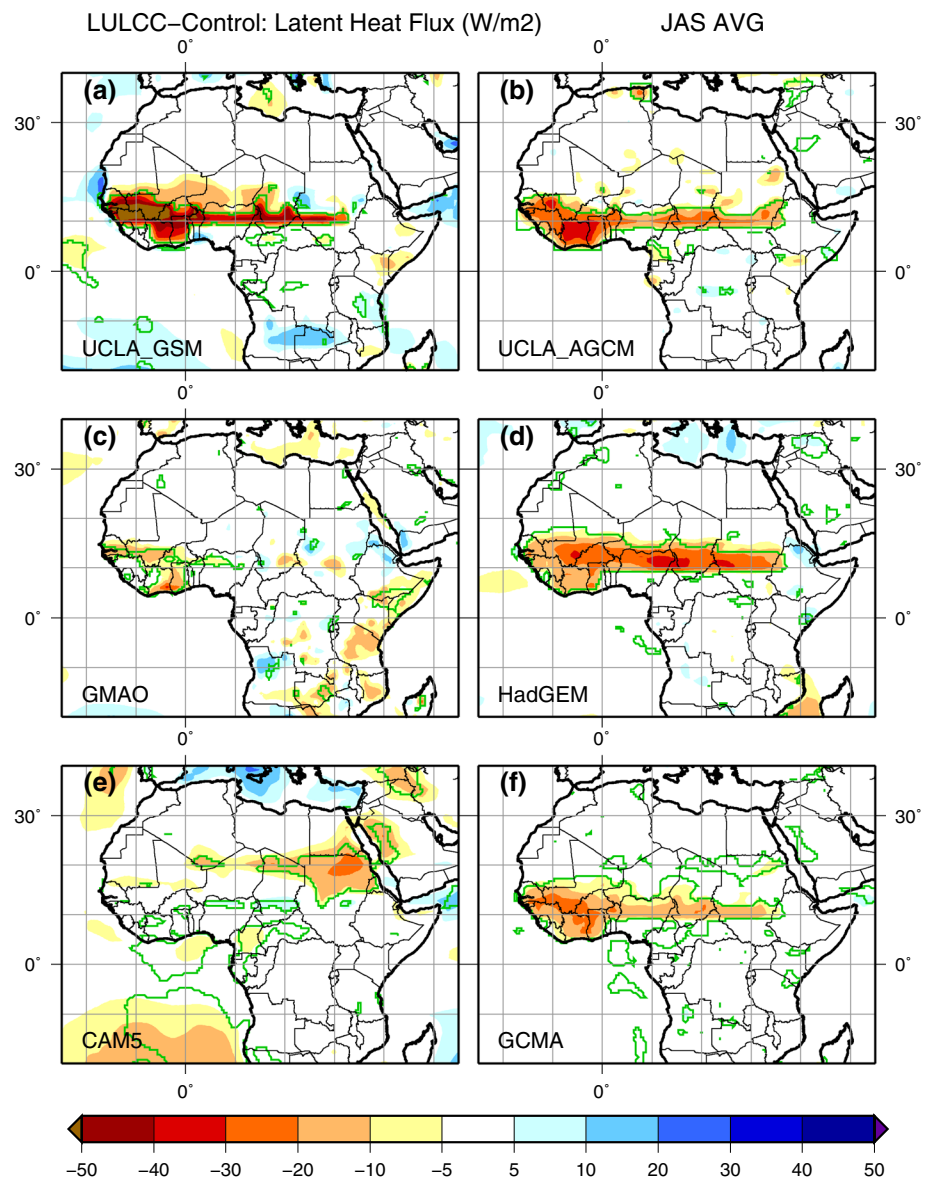
will be given below). Note that *LE* increases in a thin band from southern Mali eastward through southern Chad primarily because of slightly higher rainfall over these regions in Exp. LULCC. The *LE* is not significantly influenced by the *LAI* since it is only slightly reduced in this region for this model. The GCMA *LE* reduction is statistically significant over vegetated regions. The NT05 and NT10 *p* values (Table 4) for *LE* are less than or equal to 0.05 for all of the five of the GCMs and the GCMA, which indicates they are significant. Thus, the impact on LE is strong among all of the models. Three of the models (UCLA-AGCM, GMAO and HadGEM) produce an east–west band of *H* decreases along the northern Sahel (Fig. 8) where little to no rainfall occurs, which results mainly from the reduction in *Rnet* (compare Figs. 6, 8). Thr UCLA-GSM has a similar feature, but it is considerably smaller in area (over the easter

Sahel) but still statistically significant at the 95 % confidence level. In CAM5, a small zone of *H* increases in the northern Sahel is related to decreases in *LE*: again, this results is primarily due to a notable southward shift of the WAM in the LULCC run so that *H* increases are mainly caused by decreased rainfall:changes in the turbulent fluxes are mostly confined to the northern fringe of the LULCC zone. The GCMA *H* reductions along the northern Sahel and increases to the south are statistically significant at the 95 % confidence level. The NT05 *p* values (Table 4) for *H* are quite significant for four of the five models (≤0.01). The HadGEM model results are the exception, with *p* values which are just within levels showing significance. This is consistent with the fact that the changes in available energy (caused by the largest albedo increase among the models) at the surface translate mostly into *LE* changes

Fig. 8 As in Fig. 6, except for surface sensible heat flux, *H* (W m^{-2})

LULCC–Control: Sensible Heat Flux (W/m2)   JAS AVG
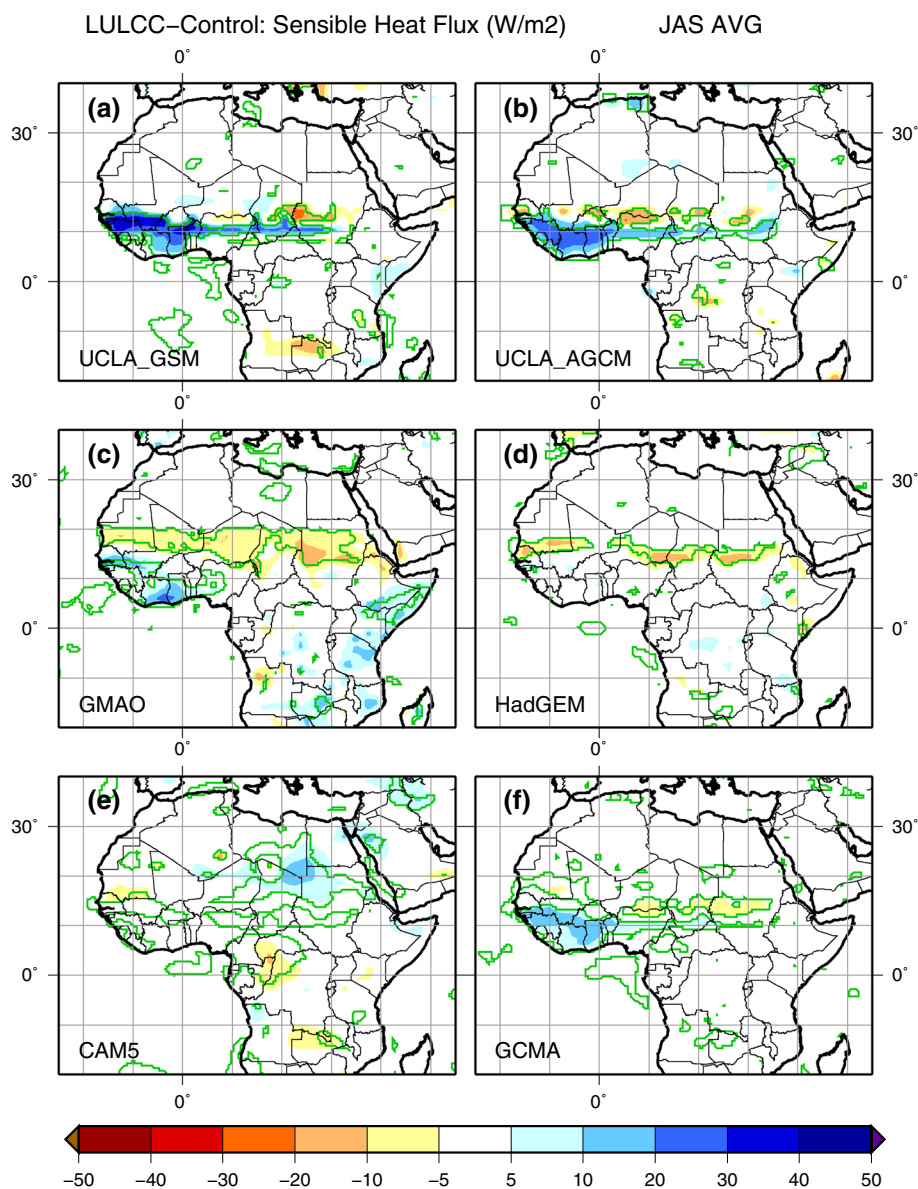
for this model. This is also reflected in the near surface air temperature *p* values (Table 4): only the HadGEM does not have significant *p* values owing to relatively little increased sensible heating of the lwoer atmosphere owing to LULCC. Values of the relative changes in the JAS surface fluxes averaged over the LULCC zone (Fig. 1) are shown in Table 2 (note that the results in the last 2 rows will be discussed in Sect. 3.4). The *LE* and *Rnet* values decrease for all five models when LULCC is imposed. The *Rnet* reductions are proportional to the albedo increases (Fig. 4). The *LE* relative reductions are between 16 and 28 % for three of the models (UCLA-GCM, UCLA-AGCM and HadGEM). The *H* increases for the two UCLA models owing to the significant effect of the decrease in vegetation coverage and density, while in the HadGEM, *H* slightly decreases since this model is dominated by the largest *Rnet* reduction. The

CAM5 and GMAO models have a less significant impact of LULCC on *H*. Finally, the *Rnet* changes are significant (NT05 *p* values at or below 0.03) for all of the GCMs (Table 4). The CAM5 NT10 *p* value (0.10) is the least significant among the models, and the corresponding area of the analysis domain is considerably smaller (at least half the size of the next closest model) than that for the other models, thus the albedo change impact is less in this GCM.

In order to better understand the impact of the surface parameter changes on the fluxes, the JAS average latent heat flux, *LE*, change verses the *LAI* difference (LULCC less the CTL value) within the LULCC zone is shown in Fig. 9. The linear regression fit is shown (red line), and the corresponding residual standard error (RSE: mm day^{-1}) and the correlations are shown in Table 3. All of the listed correlations are statistically significant to a *p* value <0.01

Table 2 Relative difference (%) between the LULCC and CTL experiments of the JAS average rainfall and surface fluxes for each GCM

GCM	Rainfall	Rnet	LE	H
UCLA-GSM	−24	−10	−28	+12
UCLA-AGCM	−20	−7	−16	+5
GMAO	−4	−5	−5	−5
HadGEM	−25	−13	−23	−3
CAM5	−17	−3	−4	+2
GMAO-w	+1	0	+2	−1
HagGEM-w	−3	−6	−6	−7

The values have been spatially averaged over the LULCC domain

Differences are between the LULCC less the CTL experiment values

Units: percentage

Rnet, LE and H represent the net radiation, latent heat and sensible heat fluxes, respectively

Reference area: LULCC area enclosed by a contour in Fig. 1

The last two rows correspond to sensitivity runs by two models with a weaker LULCC impact on the biogeophysical parameters of the land surface model (see Sect. 3.4)

(two tailed probability) except for the correlation between LE and albedo for the CAM5 model. Note that the UCLA GCMs use only a few discrete values of *LAI*, therefore the meaning of a correlation is more ambiguous for this variable, but there is a fairly linear relationship. The *LAI* reduction tends to be lowest in the northern part of the LULCC zone, where evapotranspiration tends to be lower (owing to lower *LAI* but also to less rainfall). The linear regression slopes are similar (ranging from 0.21 to 0.39) in four of the five models. This implies that a significant portion of the evaporation is from the vegetation. However, the scatter is likely due to the fact that bare soil evaporation is non-negligible, especially for tile schemes, and owing to the influence of precipitation on *LE*. The UCLA models also have the largest *LAI* decreases: UCLA-AGCM has the highest correlation between *LE* and *LAI* changes (0.88) and the second lowest value of RSE (indicating relatively little scatter about the linear fit). In contrast, the UCLA-GSM has a moderate value for correlation, but the largest RSE among the models. For the CAM5 model, a good deal of the rainfall falls in regions with little vegetation in the CTL run,

Fig. 9 The change (LULCC less the CTL values) in the JAS average latent heat flux difference (*dLE*; W m^{-2}) verses the corresponding change in *LAI* (m^2 m^{-2}) for all grid points within the LULCC zone (Fig. 1) for each GCM. Regression lines are shown in *red*, and the slope and intercept are given
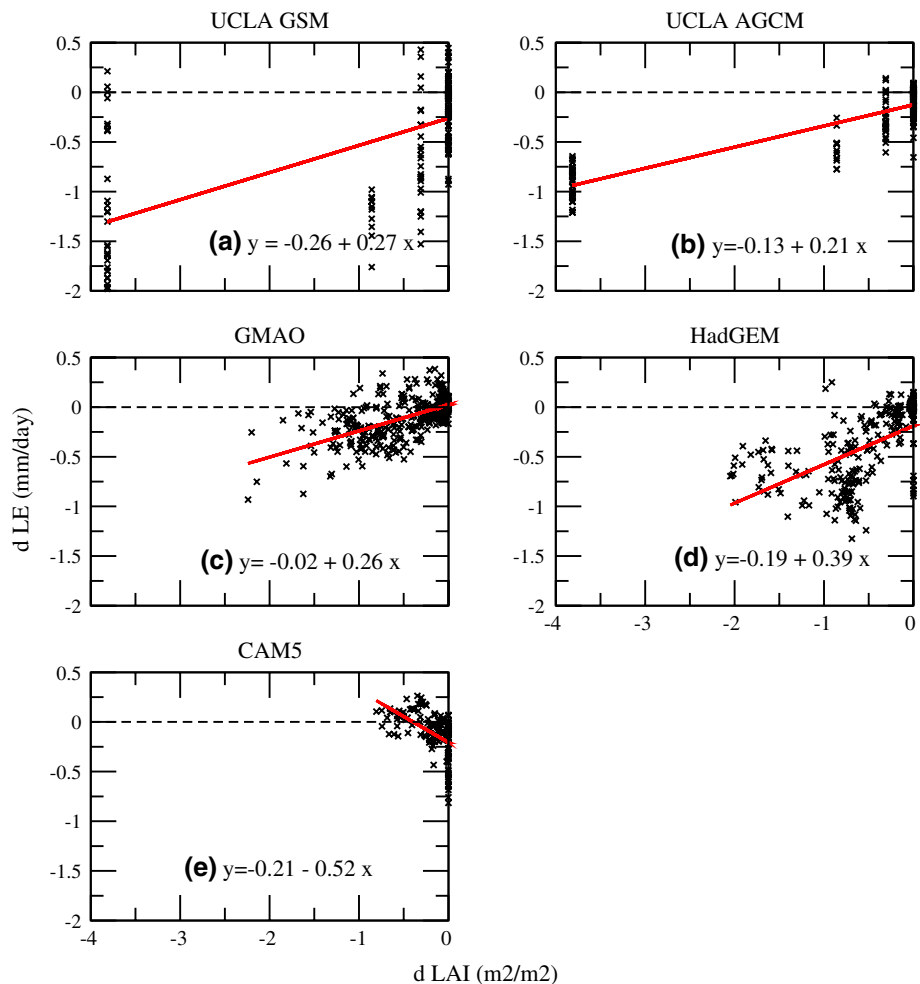
Table 3 The correlation and the residual standard error (mm day^{-1}, in parentheses) between changes in each of the two JAS averaged variables, and between rainfall and evapotranspiration within the LULCC zone

GCM	LE versus LAI	LE versus albedo	Rainf versus LAI	Rainf versus albedo	Rainf versus LE
UCLA-GSM	0.61 (0.51)	−0.88 (0.31)	0.29 (1.09)	−0.63 (0.82)	0.71 (0.76)
UCLA-AGCM	0.88 (0.16)	−0.87 (0.18)	0.65 (0.86)	−0.67 (0.93)	0.64 (0.77)
GMAO	0.64 (0.14)	0.27 (0.19)	0.58 (0.48)	0.37 (0.57)	0.59 (0.46)
HadGEM	0.55 (0.31)	−0.92 (0.14)	0.46 (0.48)	−0.84 (0.27)	0.88 (0.22)
CAM5	−0.53 (0.18)	0.03 (0.21)	−0.57 (0.61)	−0.37 (0.56)	0.25 (0.73)

Variables are listed in the uppermost row

Also refer to Figs. 11–12 and 15–16

All of the correlations listed are statistically significant for a p value <0.01 (two-tailed probability) except for the correlation between LE and albedo for the CAM5 model

LAI represents Leaf Area Index, LE represents latent heat flux, and Rainf represents rainfall

Model acronyms are given in the leftmost column

Fig. 10 The change in the JAS average latent heat flux difference (*dLE*; W m^{-2}) verses the corresponding change in albedo for all grid points within the LULCC zone (Fig. 1) for each GCM. Regression lines are shown in *red*, and the slope and intercept are given
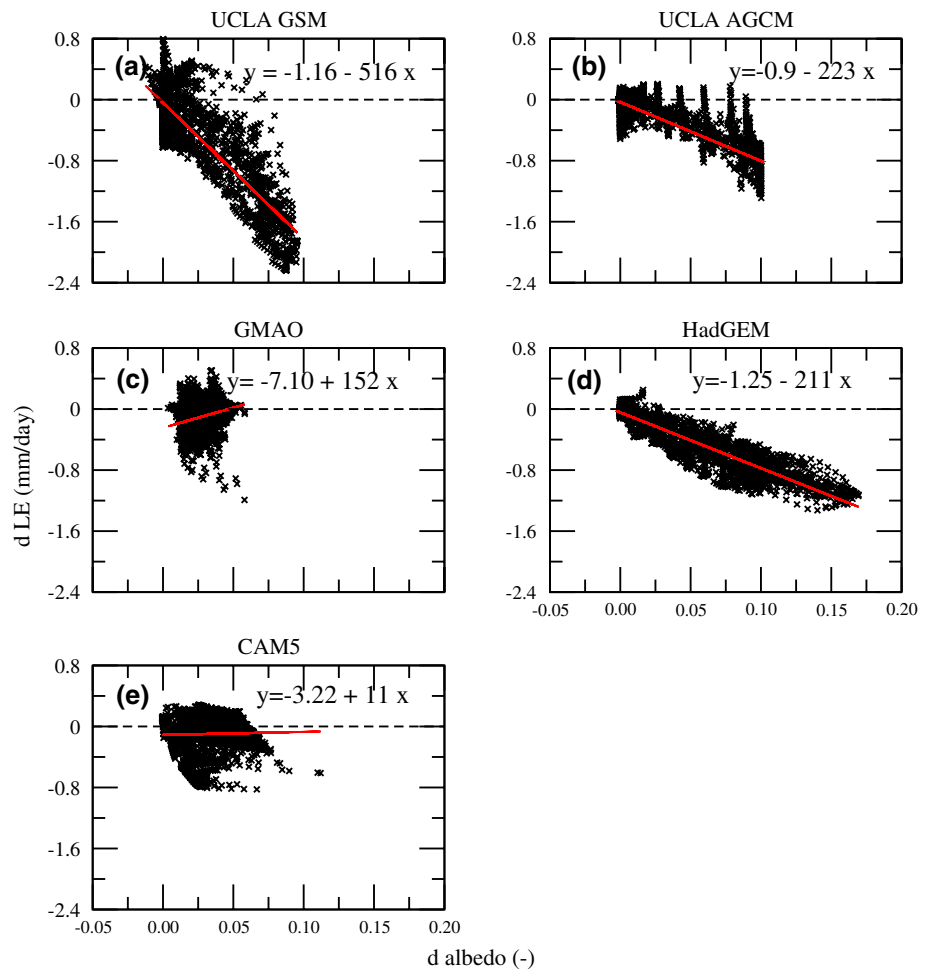
but, there is more rainfall coincident with vegetation owing to the southward shift of the monsoon in the LULCC run. These factors lead to a negative correlation. The HadGEM shows a weaker link between *LAI* and *LE* as seen by the relatively low correlation and large RSE.

The relationship between JAS *LE* and albedo is shown in Fig. 10 (the corresponding RSE and correlations are shown in Table 3). The UCLA-AGCM and HadGEM models show a fairly direct link with the absolute value of the correlations exceeding 0.87 and relatively low values of
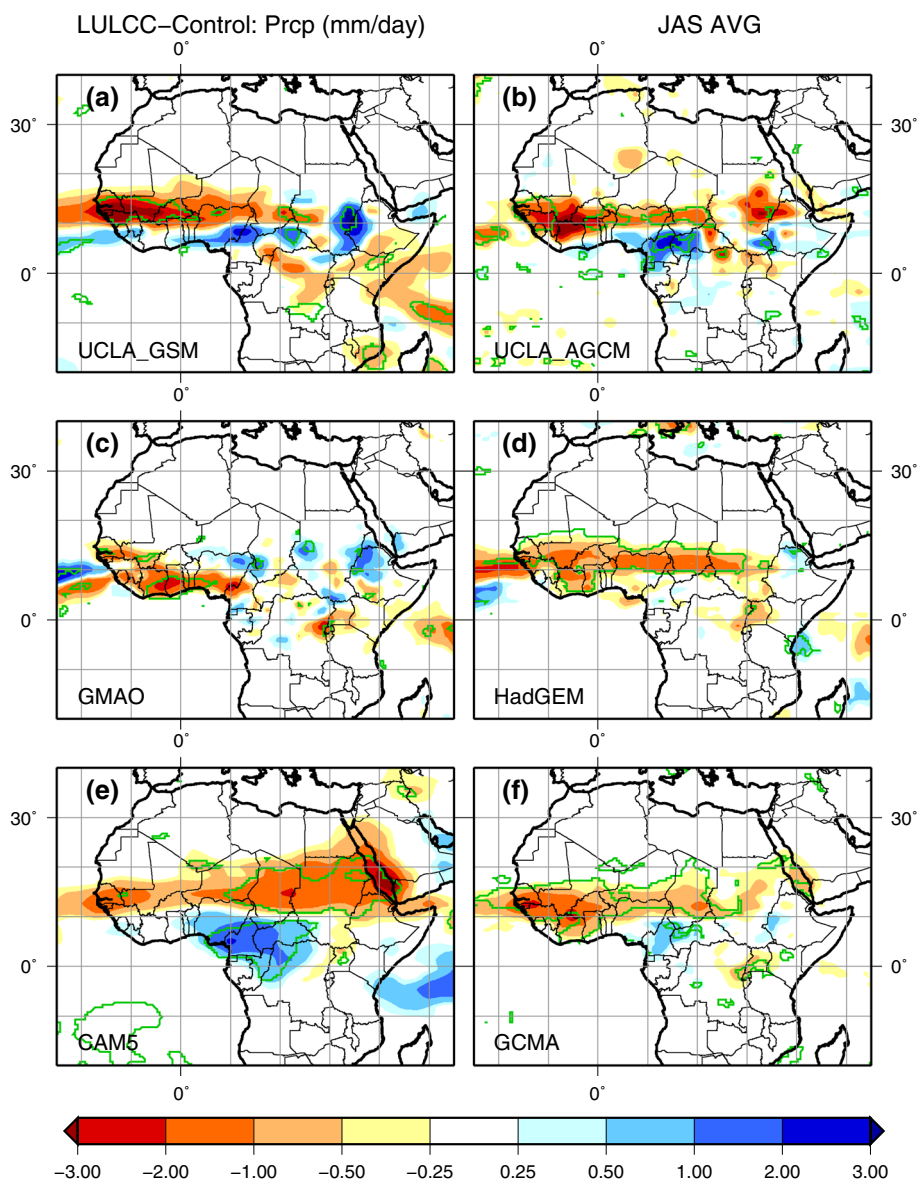
RSE (with the HadGEM having the lowest value over-
all of 0.14 mm day^{-1}). The UCLA-GSM also has a fairly
high correlation (-0.88), but with a considerably larger
RSE than the other two aforementioned models. GMAO
and CAM5 have relatively weak correlations. For GMAO,
most of the albedo changes occur northward of the region
receiving rainfall (thus with non-negligible *LE*). Thus, for
this model, the area with the maximum albedo increase is
not co-located with the area of maximum *LAI* decrease.
For CAM5, there is no appreciable relationship between
changes in *LE* and the albedo. Like *LAI*, changes in albedo
will cause changes in *LE*, which can translate into changes
in rainfall since albedo reductions are proportional to the
reduction in the surface enthalpy flux. Thus for relatively
low albedo changes, the signal is more noisy. But note that
for this model, the JAS *LE* is considerably less (roughly

half) than that for the other models within the part of the
LULCC zone receiving rainfall (see Fig. 5): this will be
discussed further in the next section. The next step is to
see how the changes in surface parameters translate to the
WAM, notably the rainfall.

3.3 Impact of LULCC on the WAM rainfall

The change in the JAS average rainfall (mm day^{-1}) and the
contours of the 95 % confidence level for a two-tailed stu-
dent *t* test for each GCM are shown in Fig. 11. The aver-
age JAS rainfall relative changes averaged over the LULCC
zone are shown in Table 2. The corresponding NT05
and NT10 *p* values are shown in Table 4. In general, the
impact of prescribing LULCC has a notable impact on the
peak WAM season rainfall. For the UCLA GCMs, rainfall

Table 4 Statistical significance testing results for the JAS average differences between the control and LULCC experiments

Variable	NT	UCLA-GSM	UCLA-AGCM	GMAO	HadGEM	CAM5	GCMA
Rainf	NT05	11.96 (0.06)	16.21 (0.01)	9.63 (0.12)	45.21 (0.03)	37.04 (0.01)	47.63 (0.01)
	NT10	22.00 (0.06)	22.67 (0.02)	15.04 (0.20)	51.38 (0.03)	46.17 (0.01)	63.63 (0.01)
Ta	NT05	44.88 (0.00)	14.42 (0.03)	23.54 (0.01)	8.88 (0.17)	34.75 (0.01)	50.92 (0.00)
	NT10	55.04 (0.00)	21.75 (0.07)	31.75 (0.05)	18.71 (0.21)	42.75 (0.01)	59.71 (0.00)
Rnet	NT05	50.04 (0.01)	39.21 (0.01)	44.22 (0.01)	62.04 (0.01)	16.00 (0.03)	83.04 (0.01)
	NT10	60.83 (0.01)	45.54 (0.01)	47.63 (0.01)	63.88 (0.01)	20.83 (0.10)	87.21 (0.01)
LE	NT05	37.96 (0.02)	35.13 (0.01)	15.88 (0.01)	53.00 (0.01)	27.25 (0.02)	63.46 (0.01)
	NT10	45.17 (0.02)	39.88 (0.01)	20.71 (0.05)	57.88 (0.01)	38.00 (0.02)	71.75 (0.01)
H	NT05	34.13 (0.01)	33.38 (0.01)	49.75 (0.01)	17.17 (0.03)	46.04 (0.00)	50.92 (0.01)
	NT10	39.54 (0.02)	39.13 (0.01)	57.13 (0.01)	23.46 (0.07)	54.00 (0.01)	58.75 (0.01)

The percentage of the points which have 5 and 10 % significance using a two-tailed student t test are indicated by NT05 and NT10, respectively. The corresponding p values are given in parentheses

Model output variables are listed in the leftmost column

The statistics computed over the domain 5–20 N and −10–30 E using the pool permutation procedure with 1000 permutations

Rainf represents rainfall, Ta represents near surface air temperature, Rnet represents surface net radiation, LE represents surface latent heat flux, and H represents surface sensible heat flux

Model acronyms are given in the uppermost row

changes are between 20 and 24 % of the total 3 month rainfall over the region with LULCC. A precipitation dipole can also been seen with large increases in rainfall over southern Niger and Cameroon, associated with a shift of the core of the monsoon rain to the south. But the area of increased rainfall which is statistically significant is very small in the two models, so the most robust signal relates to the rainfall decreases. The HadGEM also has similar rainfall decreases in the Sahel, but without a precipitation dipole. In this model, the CTL WAM core is further to the south than in the UCLA models near the southern coast of West Africa, thus the monsoon can not shift much further southward. The LULCC essentially weakens the monsoon and reduces rainfall locally (peak rainfall decreases are collocated with the reduction in *Rnet* and *LE*). The GMAO has the southernmost WAM precipitation, and the overall effect of LULCC is to weaken the peak rainfall. Note that the peak rainfall reduction is significant, 2–3 mm day^{-1}, and the area of statistical significance is collocated with the peak decrease in *LAI* (Fig. 3d). Thus, it is the change in surface fluxes leading to the change in rainfall over this region, rather than the reverse. CAM5 has the most evident dipole pattern (a significant shift of the WAM southward). Thus, the magnitude of the southward shift of the WAM rainfall in the GCMs depends on the position in the CTL experiment, i.e. the model's climatological WAM precipitation spatial distribution, and the shift is of course, limited by the southern West African coast. In all models, the overall WAM rainfall was reduced owing to LULCC (see Fig. 11f). The multi-model ensemble average rainfall change is shown in Fig. 11f, and the results are statistically

significant (to a confidence level of 95 %) for the largest areas over the central and western Sahel, and there is a smaller area over the southern portions of Ghana. A few smaller areas appear outside of the LULCC region, notably over Uganda and Kenya, but for the most part, the statistically significant reductions occur over the zone of LULCC. The NT05 p values are less than or equal to 0.03 for three of the models (UCLA-GSM, CAM5, and HadGEM) indicating significance. The UCLA-GSM p value is slightly larger at 0.06. Only the GMAO results are not significant (NT05 and NT10 p values of 0.12 and 0.20, respectively), indicative of the relatively weaker impact of LULCC. The multi-model ensemble, GCMA, is quite significant with p values of 0.01. The relatively local decreased precipitation response to reduced *LAI* is also consistent with the results of Kang et al. (2007) over West Africa.

The meridional profiles of the JAS average rainfall averaged over 2 contiguous regions (both 10° in longitude) are shown in Fig. 12. The reduction of the peak rainfall is seen in the UCLA models, especially in the western region (Fig. 12a), which is the location of the most extended (reaching the southern West African coast) and largest LULCC: the UCLA GSM and AGCM have peak reductions in rainfall of approximately 25 and 30 %, respectively, over this region. The remaining models have decreases of about 10–15 %. The CAM5 decrease is confined to the area encompassed by LULCC in the western region (Fig. 12a), but a more significant southward shift of the monsoon rains occurs to the east (Fig. 12b). The two UCLA models also show a slight southerly shift over the eastern area, but to a lesser extent than CAM5.

Fig. 12 The JAS average rainfall latitudinal profiles averaged from -10 to 0 east longitude (panel **a**) and from 0 to 10 east longitude (panel **b**). *Solid lines* correspond to the CTL simulation, *dashed lines* correspond to results from the LULCC experiment
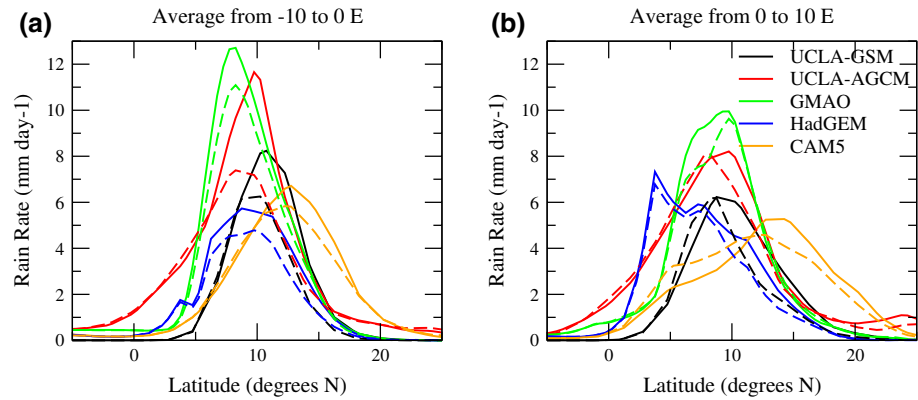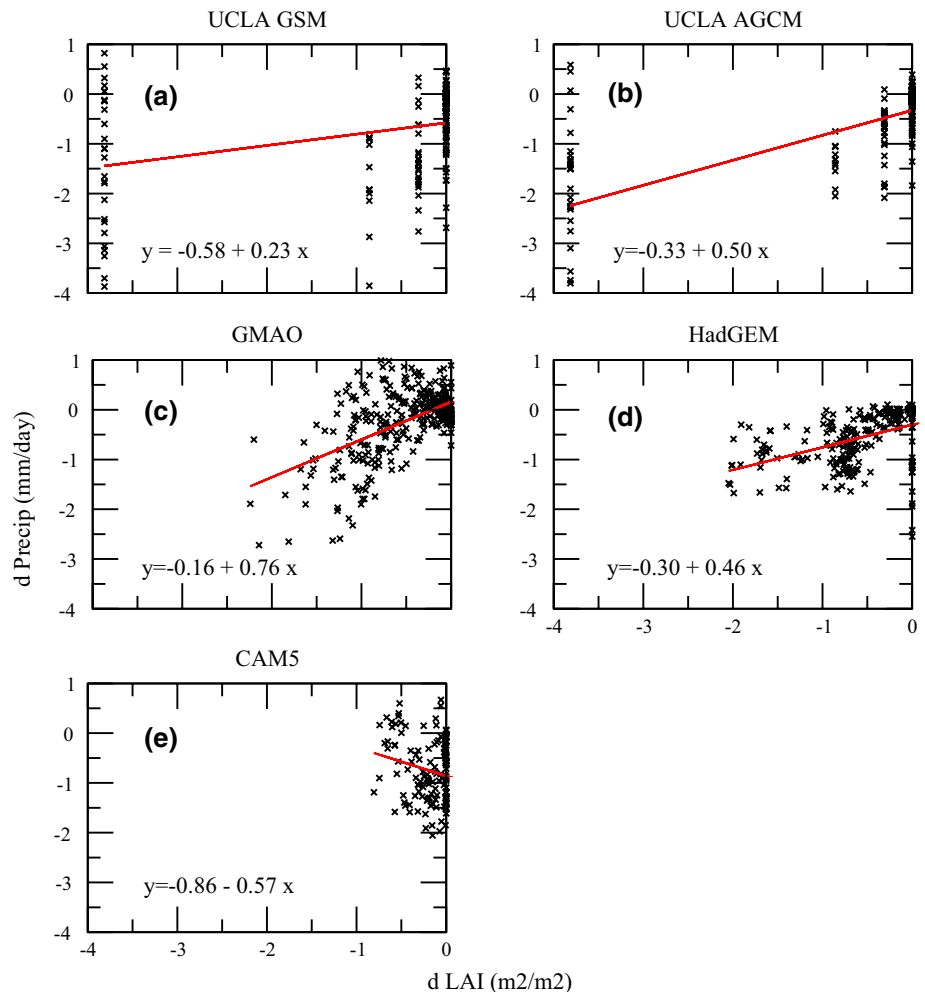

Fig. 13 The change (LULCC less the CTL values) in the JAS average rainfall difference (*dPrecip*; kg m^{-2} day^{-1}) verses the corresponding change in *LAI* (m^2 m^{-2}) for all grid points within the LULCC zone (Fig. 1) for each GCM. Regression lines are shown in *red*, and the slope and intercept are given

The GMAO peak, however, does not shift southward and there is a reduction of rainfall confined to the south of the LULCC area, again, associated with the region with the largest reduction in *LAI*. Finally, the HadGSM has a decrease in rainfall along the entire transect, but it is the largest over and just south of the area with LULCC. Nicholson and Grist (2001) studied the rainfall anomalies from 1920 to 1997 and identified four modes, two each for wet and dry conditions in the Sahel. Relatively dry years without a dipole pattern correspond to a weakening of the monsoon intensity, while those years with a dipole pattern correspond to a southward shift of the monsoon. A rainfall anomaly dipole pattern is seen in three models (UCLA-GSM, UCLA-AGCM and CAM5: Figs. 11, 12) with a

Fig. 14 The change (LULCC less the CTL values) in the JAS average rainfall difference (*dPrecip*; kg m^{-2} day^{-1}) verses the corresponding change in albedo for all grid points within the LULCC zone (Fig. 1) for each GCM. Regression lines are shown in *red*, and the slope and intercept are given
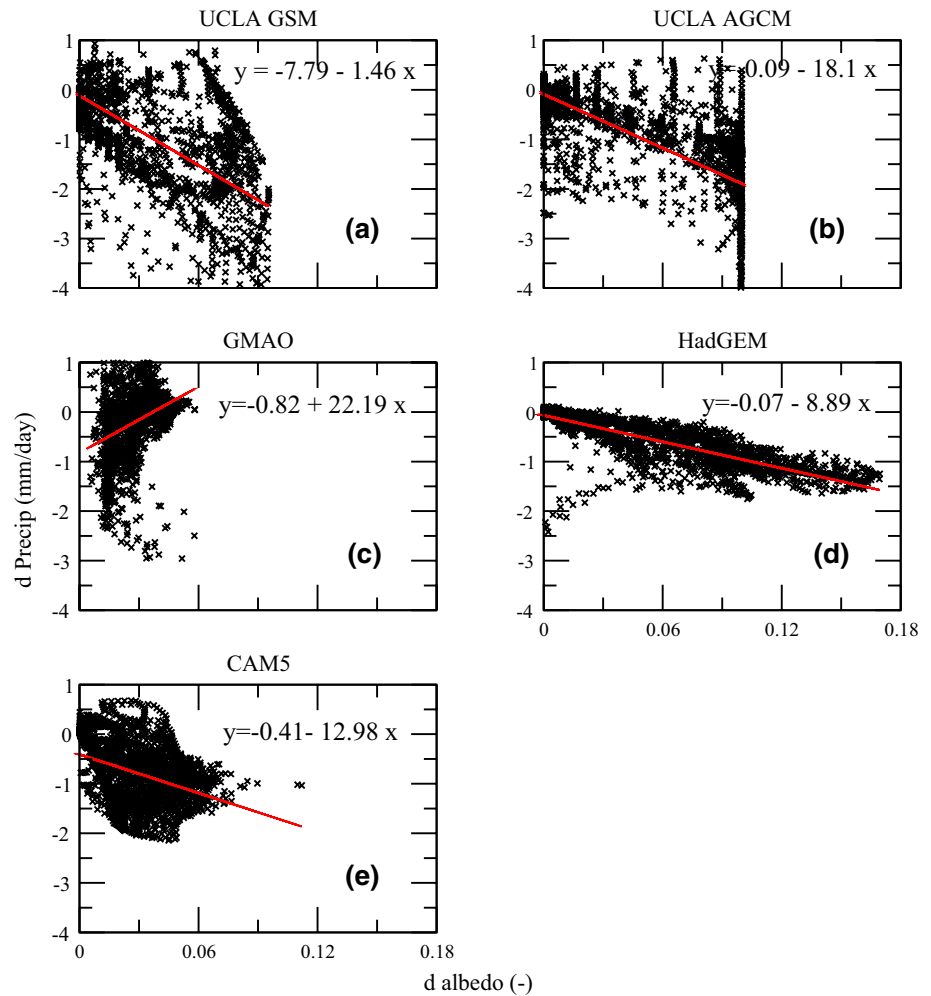

latitudinal shift similar to the findings of Nicholson and Grist (2001), however, it is only statistically significant for the CAM5 model (Fig. 11). The multi-model ensemble shows a statistically significant weakening over most of the LULCC region (Fig. 11) with only a weak rainfall anomaly dipole which is not statistically significant.

The next step is to examine any relationship between the surface parameter and rainfall changes in order to see how changes in surface fluxes translate to the atmosphere. The relationship between, *dRainf*, and *dLAI* is shown in Fig. 13 (the RSE and correlations are shown in Table 3). The correlations between *dLE* and *dLAI* (Fig. 9) are, as expected, lower and the RSE is larger since the effect is more indirect. The UCLA-GSM has a considerably weaker correlation and larger RSE, however, there is a more significant relationship for this model with the albedo change. The UCLA-AGCM has a higher correlation (0.65): since the land surface models and physiography are the same between these two GCMs, this implies that rainfall changes are co-located with *LAI* changes more owing to atmospheric processes. The GMAO and HadGEM models have the lowest RSE,

but fairly moderate correlations of 0.58 and 0.46, respectively (with slightly lower correlations compared to those between *dLE*, and *dLAI*). In contrast to the other four models, CAM5 has a negative correlation (as is also the case for *dLE* and *dLAI*, with nearly the same values). This results primarily because the monsoon shifts southward for this model (so that biogeophysical parameter changes are not co-located with rainfall changes). In terms of the relationship between *dRainf*, and *d*albedo (Fig. 14), the UCLA-GSM and UCLA-AGCM models have the largest RSE, but moderate values of correlation (−0.63 and −0.67, respectively). Note that the HadGSM has the lowest RSE and the largest (negative) correlation (−0.84) between *dRainf*, and *d*albedo, which is consistent with the analyses presented in the previous sections. GMAO has among the lowest correlations (0.37) among the models which is also positive (in contrast to the other models), and this is primarily due to albedo changes occurring mainly outside the region of active rainfall. CAM5 has a correlation of the same sign as the other four models but a relatively low value (−0.37) owing to a more spatially heterogeneous change in albedo

Fig. 15 The change (LULCC less the CTL values) in the JAS average rainfall difference (*dPrecip*; kg m^{-2} day^{-1}) verses the corresponding change in evapotranspiration, *Evap* (kg m^{-2} day^{-1}), for all grid points within the LULCC zone (Fig. 1) for each GCM. Regression lines are shown in *red*, and the slope and intercept are given
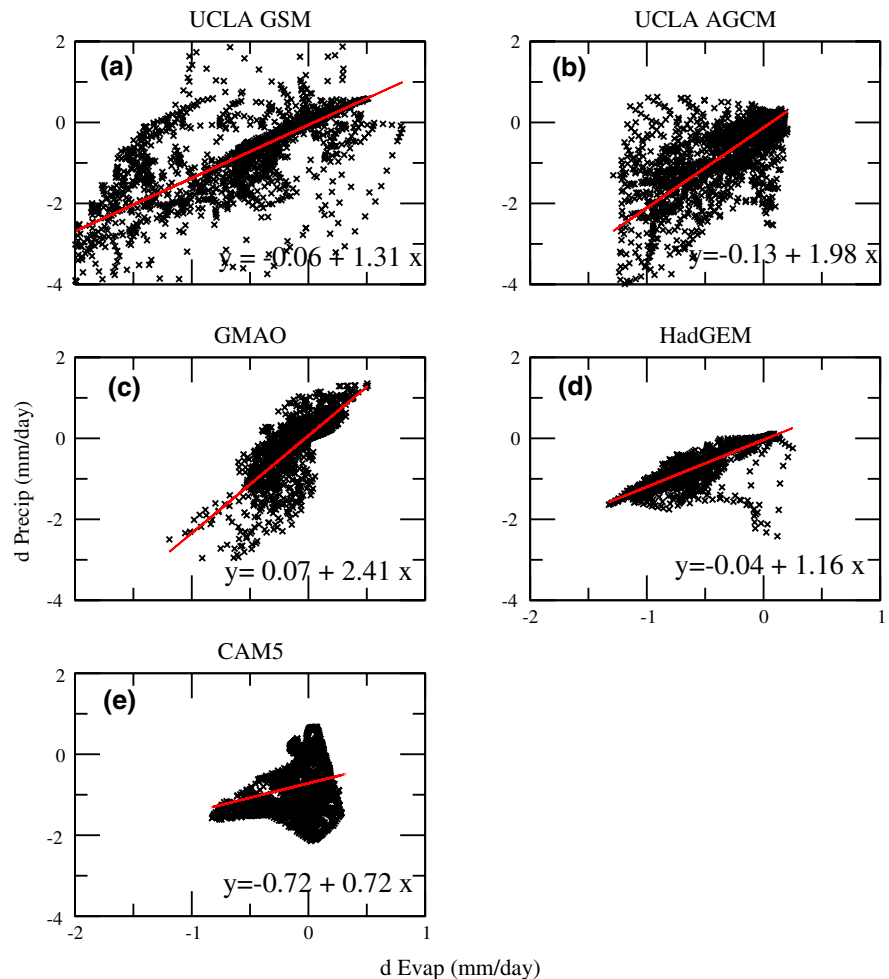
(along with relatively lower changes compared to the other models) along with the shift in the WAM position, both of which contribute to the weaker relationship.

The relationship between *dRainf*, and *dLE* is shown in Fig. 15. As one might expect for West Africa, there is a relationship between these two variables (implying generally water-limited conditions over the region where LULCC has been imposed), however, determining cause and effect is a challenging task. It is, however, of interest to note that in three of the models (UCLA-GCM, UCLA-AGCM and GMAO), precipitation decreases are 30 to over 100 % larger than the corresponding evaporation decreases. Therefore, the reduction in *LE* has a significant influence on the moisture convergence for these models. In the HadGEM model, the RSE is by far the lowest among the models and the slope of the regression is close to one. Since the change in surface albedo (which dominates the *Rnet* change) explains most of the *LE* change, then this implies that *d*albedo (via *dLE*) is the main factor causing the *dRainf*. In contrast, GMAO precipitation changes owing to both *dLE* and *dLAI* are very consistent in terms of both RSE and correlation, although the decreases in precipitation are more

than double those seen in *LE*, thus the feedback mechanism is more complex. CAM5 has among the largest RSE values and the lowest correlation owing to a generally lower magnitude impact of LULCC on the biogeophysical parameters and the less local nature of the changes (the shift of the monsoon). Thus, even though the impact on the rainfall is less than for the other GCMs in the absolute sense, small changes in the LULC cause a large shift in the monsoon location for this model. Thus the impact seems to be less local in this model than in the others.

The meridional gradients of the surface turbulent fluxes, which are modulated by the near-surface conditions, are intimately tied to one of the key features of the WAM: the AEJ (e.g. Cook 1999). The impact of LULCC on the air temperature and zonal winds is shown in Fig. 16. The JAS average air temperature and zonal component of the wind speed (*u*) have been averaged over the longitude band from −10° to 10° E, and are shown as a function of pressure and latitude. Temperature changes (LULCC-CTL values) are color contoured. The impact of LULCC is most readily seen as a warming of the lower atmosphere in four of the five models (Fig. 16a–d), but the magnitude
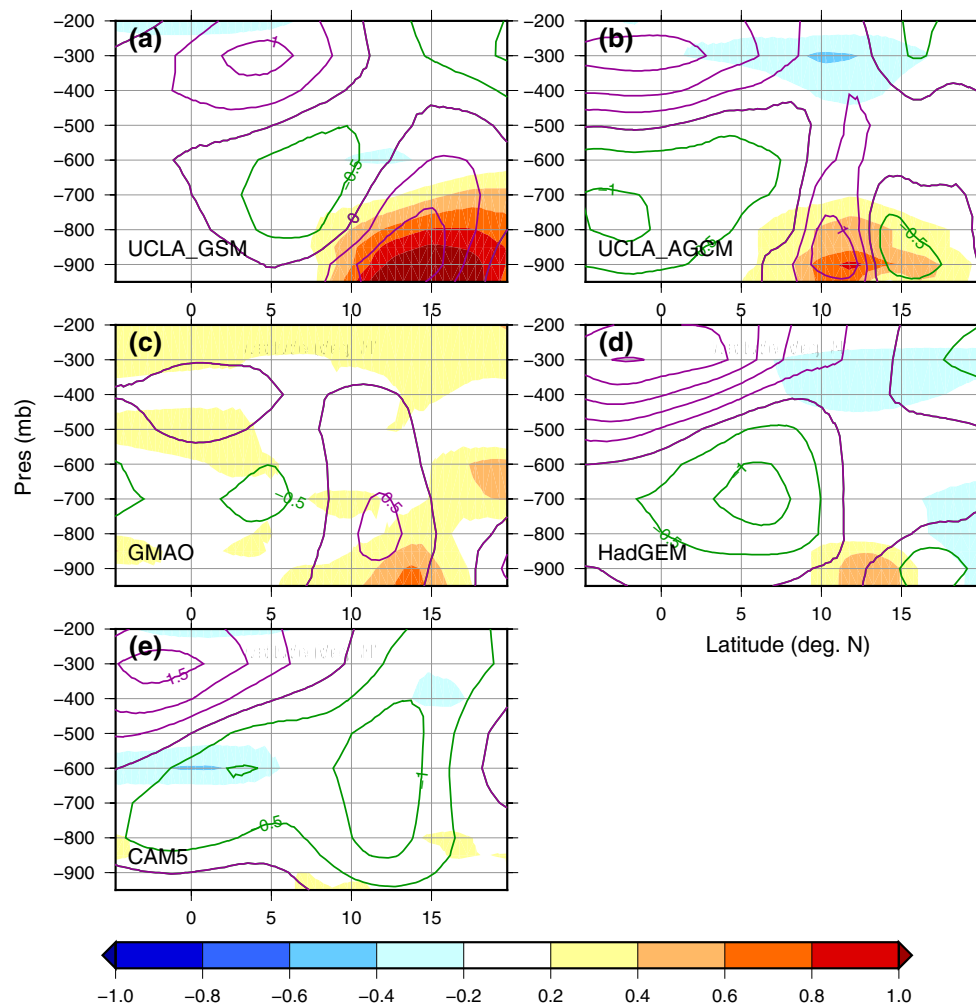
Fig. 16 The JAS average u wind component and air temperature changes (LULCC-CTL runs) as a function of pressure and latitude (averaged in longitude from −10° to 10° E). Air temperature changes are color filled (using the scale indicated here), while changes in the zonal wind are indicated using contour lines (contours are in m s^{-1}, and *green colors* represent an increase in easterly wind flow)

differs considerably among the GCMs. The largest warming occurs for the models with the most significant *LAI* decrease in this region (the UCLA GCMs). As mentioned previously, despite the larger albedo under LULCC, the reduction in *LAI* (and corresponding increase in the Bowen ratio) has resulted in a statistically significant increase in *H* for these two models (Fig. 8a, b) over this region. The GMAO model also has a statistically significant increase in *H* (Fig. 8c), but since *LAI* changes are relatively less than that for the UCLA models (compare Fig. 3a, b), the *H* increases are lower leading to less atmospheric warming. The HadGSM has relatively small increases in *H* (<5 W m^{-2} on average) and thus the warming (Fig. 16d) is the least among the four aforementioned models. And the modest increases in *H* were not statistically significant for this model. Finally, the CAM5 model changes in *H* are so weak such that there is essentially no warming of the

lower atmosphere in this region. Again, the behavior of this model is quite different from the others owing to the CTL position of the monsoon. Thus, the only models which show warming and are statistically robust in terms of *H* are the UCLA and GMAO models. Newell and Kidson ([1984]) showed that for years with relatively dry (and warm) conditions over the Sahel, the easterly winds between 850 and 700 hPa typically increase over this region (−10–10 E) between 0° and 20° N latitude. However the simulated differences here are considerably smaller than those reported in Newell and Kidson ([1984]) for the month of August by up to several m s^{-1}. In addition, Nicholson ([2008]) showed that the AEJ is shifted southward for relatively dry years. The three models with statistically significant *H* increases show a dipole pattern in the *u*-component wind change (Fig. 16a, b) which is consistent with a southward shift in the AEJ, although again, the wind speed changes are

Fig. 17 As in Fig. 11, except for the two sensitivity tests with reduced LULCC impact on the biogeophysical parameters (see Fig. 4)
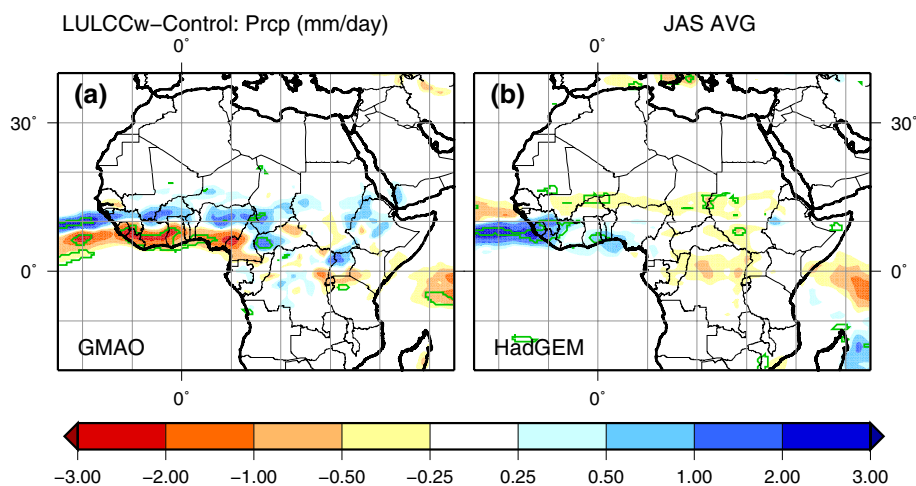
relatively modest. Newell and Kidson (1984) also show an increase in upper level westerlies, and both UCLA models show increases with peak values on the order of 1–2 m s^{-1} south of 5°–10° N at about 300 hPa, which is consistent with the Newell and Kidson (1984) 200 hPa analysis. The HadGSM also shows both the low and upper level features, but because the warming in the lower atmosphere is not linked to a statistically significant increase in H, we have less confidence in this result. Finally, the CAM5 model is similar with respect to the upper level winds, however, the other features (heating and lower level winds) do not fit this model. Thus, only two models (UCLA) have both the lower and upper level difference features described by Newell and Kidson (1984) for a relatively dry year and the strongest lower atmospheric warming resulting from statistically significant H increases. These two models have the most significant impact on albedo and LAI, thus, it seems a certain threshold of LULCC is required to obtain a signal in terms of the atmospheric circulation, and this signal is consistent with relatively dry years.

3.4 Sensitivity tests

The discussions above show that although the models have substantial differences in their response to the LULCC, they show a general agreement that LULCC which occurred over the prescribed time period has a positive impact on Sahel drought. In previous LULCC multi-model studies, it has been shown that models have difficulties reaching a consensus view of the impact, part of which is due to the difficult task of prescribing LULCC in a consistent manner among different models (Pitman et al. 2009). A similar situation was faced in the early phases of this experiment. In the initial simulations with GMAO and HadGEM, the vegetation type changes based on the classification tables in their respective models only resulted in relatively small changes in one or more of the three key biogeophysical

parameters (notably LAI and albedo) which were significantly less compared to the other GCMs, despite adherence to the WAMME guidance. As an example, the initial albedo JAS changes for GMAO and HadGEM are shown in Fig. 4c, e, respectively (compared to the final values for a stronger impact of LULCC shown in Fig. 4d, f, respectively). In this section, results from the simulations for GMAO and HadGEM using the parameter values corresponding to a weak change in biogeophysical parameters are presented and compared to those corresponding to the stronger changes used in the analysis presented in Sects. 3.1–3.3. The main goal of these experiments is to highlight that the application of a common protocol for LULCC can induce big differences in the atmospheric response if the biogeophysical impact is not similar despite the appearance that the models had similar LULCC.

The experiments with the relatively weak change in vegetation parameters are labeled as LULCCw. The average JAS rainfall differences between Exp. LULCCw and Exp. CTL are shown in Fig. 17 (as a reference, compare to Fig. 11c, d). In addition, the rainfall change averaged over the LULCC zone for these two models are shown in the last two rows of Table 2 (labeled GMAO-w and HadGEM-w). The main difference between the GMAO LULCC and LULCCw model runs is that the albedo is almost unchanged in the central and northern Sahel (Fig. 4c) and the LAI is slightly decreased. In the northern Sahel, the relatively small decreases in LAI with no appreciable decrease in albedo leads to an increase in rainfall compared to the CTL case owing to an increase in sensible heating leading to more convection. In contrast, to the south (where water stress is significantly less), the relatively larger decrease in LAI leads to lower evapotranspiration and moisture convergence, thus less rainfall. The result is a precipitation dipole, which is the opposite of the other models but is more related to a longitudinal flattening (weaker meridional gradient) of the monsoon rains than a southward shift

in this model. But as in the LULCC experiment, the only region with a statistically significant change (at the 90 % confidence level) is over southern Ghana where the LAI change is the largest (Fig. 17a). The overall rainfall change within the zone of land cover change is essentially offsetting: the JAS LULCCw-domain averaged rainfall changes (increases) by only 1 % (Table 2). For the HadGEM, it was shown in the previous section that the reduction in *Rnet* (albedo) directly reduced the *LE* and the rainfall (by nearly one-to-one). In the LULCCw experiment, the albedo change was substantially weaker than in the default LULCC simulation. This resulted because the soil albedo was prescribed using present day observations, which were then inconsistent with the vegetation degradation. The main impact of this difference is that there is almost no change to the rainfall (a JAS LULCCw domain average decrease of 3 %, compared to 25 % in the LULCC run: see Table 3). This result is entirely consistent with the close coupling between *Rnet* and rainfall found for this model. There is a thin band of reduced rainfall along the north-central Sahel. In this region both the sensible and latent heat fluxes are slightly lower, which seems to be mainly a result of the lower vegetation density. But the biogeophyiscal parameter change is sufficiently weak in the LULCCw experiment so that there is virtually no statistical significance (at the 95 % confidence level) within the Sahel (Fig. 17b). These results underscore how LULCC impacts different LSM parameters, and then can potentially have a significant impact on a coupled system, such as the WAM.

4 Discussion and conclusions

The goal of the present study is to explore the impact of LULCC on the WAM using a strong but feasible degradation methodology with a suite of five GCMs. The overall impact of LULCC on the WAM for the 5-year simulation herein can be summarized as follows:

1. Reducing the *LAI* increases the Bowen ratio in regions where transpiration and evaporation from intercepted canopy water are occurring. In all of the regions where *LAI* (and evaporation) decreases (above some relatively low threshold), the rainfall also decreases. This response is common to all the models. Therefore in such regions, resulting decrease in *LE* is the main cause for reduced rainfall, rather than the reverse.

2. The increase in albedo reduces the net radiation, thus the energy available for the turbulent surface fluxes are also decreased, but the partitioning of this energy loss is modulated by the *LAI* change. In models with moderate *LAI* changes, latent heat flux is reduced during the wet season in regions receiving rainfall. For models with large *LAI* changes, the reduction in latent heat can exceed the reduction in net radiation caused by the albedo change (owing to large changes in Bowen ratio), thus the sensible heat flux increases. In the dry season or in dry regions (north of the area receiving rainfall), the increase in albedo (reduction in surface net radiation) translates nearly directly into a decrease in sensible heat flux (and there is little to no impact on overall monsoon rainfall).

3. The model specific simulated WAM location influences the impact of the LULCC. The models with the WAM (defined here as the zone with peak JAS rainfall) located furthest to the north (CAM5) experienced a shift in the overall monsoon position owing to LULCC. This feature is seen as a statistically significant (at the 95 % confidence level) JAS precipitation difference dipole pattern. Two other models (with monsoons located further south) also had a dipole pattern, but rainfall increases were not statistically significant. But the main (and statistically robust) impact in all of the models is a lowering of monsoon rainfall within the LULCC zone: the CAM5 was the only model for which this effect extended outside of this zone (to the north). For the models with a more southerly peak monsoon rainfall (HadGEM and GMAO), there was essentially no southward shift and only a rainfall reduction.

4. In this WAMME study, the goal is to favor consistent changes in the values of the biogeophysical parameters over changes in a particular model's LULC, since how vegetation classes and their associated parameter values are defined can vary tremendously between different models. Collaborations were engaged with each modeling group in order to ensure the LULCC experiment not only had a consistent change in the spatial distribution of LULCC and the vegetation types, but also in terms of the vegetation characteristics and parameters, which provide the real forcing at the land surface in the LULCC experiment. But despite these efforts, this remains a challenging task mainly owing to how LULC and the associated biogeophysical parameters are defined in the models.

The impact of LULCC in a single GCM can be quite different from other models in this region owing to several factors. The first is the simulated WAM intensity and location. Most GCMs have continued difficulties simulating the spatial dimensions, temporal evolution, triggering and strength of these systems (e.g.s Hourdin et al. 2010; Roehrig et al. 2013). These results highlight the need for improved multi-model experiments in order to progress on the understanding of LULCC, and for further improvement of the simulation of monsoon systems. In the WAMME I

experiment, substantial evaluations of the WAMME models' performance in simulating the WAM and the surface energy and water balances were made (Xue et al. 2010a; Boone et al. 2010), which provide the base for the WAMME II experiment. The second factor is that the coupling strength is known to be highly variable among models for the same region (Koster et al. 2004), and there is a need to improve the understanding of land/atmosphere interaction using observations (Dirmeyer et al. 2009; Taylor et al. 2012a, b). This region has been highlighted as a region with strong surface-atmosphere coupling (Xue et al. 2010b) since it is in a water-limited transition zone (between arid and wet regions) with a considerable convective rainfall component, and thus it is not surprising that the modeled WAM is sensitive to changes in the surface properties. The third factor is how LULCC is applied (in a relatively consistent manner for multiple models), and how a given LULCC impacts the biogeophysical surface parameters. In broad agreement with the findings of Pitman et al. (2009) and de Noblet-Ducoudré et al. (2012), the effect of LULCC varies considerably among the models, even though an attempt has been made to harmonize the LULCC as much as possible by selecting a relatively simple implementation. LSMs tend to have highly model specific physiographic databases, which have been implicitly tuned to some extent within coupled model systems to the extent that swapping physiographic databases between two different LSMs will likely lead to different climatological features in coupled GCM models. Also, the different approaches to representing the surface features (dominant class, aggregated parameters, explicit tiles for each class present in a GCM grid cell, and the number of classes) can lead to differences in the strength of LULCC for a given grid cell or region. For example we found that the dominant class schemes have a more dramatic LULCC effect than seen in the tile schemes. This underscores the importance of the LSM (and LULCC) implementation.

The present study shows that the LULCC change induces a mostly local effect consistent with the findings of Pitman et al. (2009), as seen in the correspondence between evaporation, net radiation and the precipitation. The first order impact of LULCC was to change the surface fluxes within the LULCC zone, as expected. All of the models had statistically significant changes in surface fluxes over the region of LULCC at the 95 % confidence level. However, the degree to which each of the fluxes was affected varied among the models. For one model, HadGEM, the albedo changes translated directly into an evapotranspiration reduction, which directly impacted (reduced) the rainfall. In two other models (UCLA-GCM and UCLA-AGCM), the albedo reductions again resulted in reduced latent fluxes, but these were co-located with *LAI* reductions that translated into increased sensible heat flux. In the GMAO model,

the biggest albedo changes occurred outside of the main area receiving monsoon rainfall, thus *LAI* changes were the biggest factor in reducing rainfall. The albedo increase seemed to have relatively little impact when it occurred north of the area receiving rainfall. Three of the models had precipitation dipole patterns related to a decrease in rains within the LULCC zone and a smaller area of increases with a peak located over Cameroon. But the model with the strongest and statistically robust dipole, CAM5, had a large shift of the monsoon rains to the south. This model also has a CTL core monsoon position further north than the other models, and it is the only one that shows a substantial shift in the monsoon position although the impact is still the largest within the LULCC zone. The local link between the rainfall changes and the surface fluxes is more difficult to establish for this model. But note that, as mentioned in Sect. 3.2, the *LE* is nearly half of that of the other models in the active rain area within the LULCC zone, and this flux is one of the key linkages involved in the coupling of rainfall with the surface at seasonal scale (Xue et al. 2010a; Dirmeyer 2011). Further work needs to be done to determine if this result occurs because this model has a different coupling strength with the atmosphere than the other models. The JAS average rainfall decreased over the LULCC zone (encompassing the Sahel and Ivory coast) by 4–25 % among the models owing to LULCC. The rainfall reductions were almost entirely confined to the LULCC zone except for some rainfall changes which occurred a certain distance downstream of the coast over the eastern Atlantic. This impact was found to dampen out fairly rapidly with increasing distance from the West African coast. In three of the models, the reduction in rainfall was larger than the reduction in evapotranspiration, so that the reduction in moisture convergence was considerably larger than decreases in evapotranspiration. In four of the models, an increased meridional temperature gradient in the lower atmosphere in the LULCC experiment was caused mainly by a decrease in *LAI* (corresponding with a Bowen ratio increase) generally leading to a the southerly shift of the AEJ (but again, the degree of this shift was also related to the CTL position). Thus, changes in the atmospheric circulation also play an important role (e.g. Xue 1997).

This is essentially a pilot multi-model study for obtaining a better understanding of the effects of LULCC over West Africa. A small number of GCMs, climatological SST forcing resulting in a multi-year ensemble, and a relatively simple methodology for representing LULCC were used in order to focus on elucidating the first order physical mechanisms. This study is an extension of previous LULCC studies in that special attention has been made to have a consistent biogeophysical response (in terms of land surface parameters). In addition, based on these results, it can be inferred that the use of climatological

land cover can lead to inconsistencies and errors in GCM studies for West Africa, given the high sensitivity to the surface properties in this region which have a large inter-annual variability, notably the *LAI*. Inconsistencies can also arise between locations where LULCC is imposed and those of the simulated monsoon (thereby potentially influencing the magnitude of the impact of LULCC). One way to address this issue is to use GCMs that include inter-active vegetation schemes within the LSMs (e.g., Wang and Eltahir 2000; Zhang et al. 2015), but such models are still rapidly evolving and they add an additional degree of freedom to the coupled system (it is not clear whether including such feedbacks will dampen or amplify the signal). It is suggested that future multi-model LULCC studies over west Africa include this component at least as a part of sensitivity tests. In terms of the observable impacts of LULCC, there is evidence from satellite data that the Sahel has experienced, on average, a re-greening over the last few decades, and this signal is probably mostly related to a modest recovery in rainfall (Dardel et al. 2014). However, local areas more susceptible to soil degradation (such as those characterized as shallow, sandy soils) have shown a reduction in vegetation cover. In addition, several studies have suggested that the recent expansion of irrigation in Northwest India and Pakistan could be having deleterious effects on monsoon precipitation (Douglas et al. 2009; Saeed et al. 2009; Tuinenberg et al. 2012; Guimberteau et al. 2012; Wei et al. 2013). With more LULCC data available from different sources showing substantial values in past decades (e.g. Hurtt et al. 2011; Kim et al. 2014) in addition to experience gained from previous multi-model studies (Pitman et al. 2009; de Noblet-Ducoudré et al. 2012), LULCC effects within the monsoon system can be more realistically assessed with ensemble runs in parallel with offline LSM simulations with different LULCC scenarios (ranging from weak to strong degradation) in an effort to better quantify the changes in surface parameters required to produce an atmospheric signal (e.g. Xue and Dirmeyer 2015). Finally, it is suggested that future work should be undertaken to evaluate whether the sign and strength of the feedbacks between the surface and the atmosphere simulated by large scale atmospheric models are consistent with observations (Taylor et al. 2012a, b).

References

Arakawa A, Schubert WH (1974) Interaction of a cumulus cloud ensemble with the large scale environment. J Atmos Sci 31:674–701

Blein R, Soulé BG, Dupaigre BF, Yérma B (2008) Agricultural Potential of West Africa. Economic Community of West African States (ECOWAS). Foundation pour l'agriculture et la ruralité dans le monde (FARM). pp 118

Boone A, Poccard-Leclerq I, Xue Y, Feng J, De Rosnay P (2010) Evaluation of the WAMME model surface fluxes using results from the AMMA land-surface model intercomparison project. Clim Dyn 35:127–142. doi:10.1007/s00382-009-0653-1

Charney JG (1975) Dynamics of deserts and drought in the Sahel. Q J R Meteorl Soc 101:193–202

Charney JG, Quirk WJ, Chow S-H, Kornfield J (1977) A comparative study of the effects of albedo change on drought in semi-arid regions. J Atmos Sci 34:1366–1385

Chou MI, Suarez MJ (1994) An efficient thermal infrared radiation parameterization for use in general circulation models. NASA Tech Mem 104606(3):85

Chou M-D, Suarez MJ, Liang XZ, Yan M-H (2001) A thermal infrared radiation parameterization for atmospheric studies. Technical report series on global modeling and data assimilation, vol 19, NASA/TM-2001-104606. pp 68

Cook KH (1999) Generation of the African easterly jet and its role in determining West African precipitation. J Clim 12:1165–1184

Dardel C, Kergoat L, Hiernaux P, Mougin E, Grippa M, Tucker CJ (2014) Re-greening Sahel: 30 years of remote sensing data and field observations (Mali, Niger). Remote Sens Environ 140:350–364

de Noblet-Ducoudré N, Boisier J, Pitman A, Bonan G, Brovkin V, Cruz F, Delire C, Gayler V, van den Kurk B, Lawrence D, van der Molen M, Müller C, Reick C, Strengers B, Voldoire A (2012) Determining robust impacts of land-use induced land-cover changeson surface climate over North America and Eurasia; Results from the first set of LUCID experiments. J Clim 25:3261–3281. doi:10.1175/JCLI-D-11-00338.1

Derbyshire SH (2011) Adaptive detrainment in a convective parametrization. Q J R Meteorol Soc 137:1856–1871

Dirmeyer PA (2011) The terrestrial segment of soil moisture-climate coupling. Geophys Res Lett 38:L16702. doi:10.1029/2011GL048268

Dirmeyer PA, Schlosser CA, Brubaker KL (2009) Precipitation, recycling, and land memory: an integrated analysis. J Hydrometeorol 10:278–288

Douglas EM, Beltrán-Przekurat A, Niyogi D, Pielke RA Sr, Vörösmarty CJ (2009) The impact of agricultural intensification and irrigation on land-atmosphere interactions and Indian monsoon precipitation-a mesoscale modeling perspective. Glob Planet Change 67:117–128. doi:10.1016/j.gloplacha.2008.12.007

Edwards JM, Slingo A (1996) Studies with a flexible new radiation code. I: choosing a configuration for a large-scale model. Q J R Meteorol Soc 122:689–719

Essery RLH, Best MJ, Betts RA, Cox PM (2002) Explicit representation of subgrid heterogeneity in a GCM land-surface scheme. J Hydrometeorol 4:530–545

Govaerts Y, Lattanzio A (2008) Estimation of surface albedo increase during the eighties Sahel drought from Meteosat observations. Glob Planet Change 64:139–145

Guimberteau M, Laval K, Perrier A, Polcher J (2012) Global effect of irrigation and its impact on the onset of the Indian summer monsoon. Clim Dyn 39:1329–1348

HadGEM2 model development team (2011) The HadGEM2 family of met office unified model climate configurations. Geosci Model Dev 4:723–757

Hagos S, Leung LR, Xue Y, Boone A, de Sales F, Neupane N, Huang M, Yoon JH (2014) Assessment of uncertainties in the response of the African monsoon precipitation to land use change simulated by a regional model. Clim Dyn 43:2765–2775. doi:10.1007/s00382-014-2092-x

Hansen MC, DeFries RS, Townshend JR, Sohlberg R (2000) Global land cover classification at 1 km spatial resolution using a classification tree approach. Int J Remote Sens 21:1303–1330

Harshvardhan DaviesR, Randall DA, Corsetti TG (1987) A fast radiation parameterization for atmospheric circulation models. J Geophys Res 92:1009–1016

Houldcroft CJ, Grey WMF, Barnsley M, Taylor CM, Los SO, North PRJ (2009) New vegetation albedo parameters and global fields of soil background albedo derived from MODIS for use in a climate model. J Hydrometeorol 10:183–198. doi:10.1175/2008JHM1021.1

Hourdin F, Musat I, Grandpeix J-Y, Polcher J, Guichard F, Favot F, Marquet P, Boone A, Lafore J-P, Redelsperger J-L, Ruti PM, Dell'aquila A, Filiberti MA, Pham M, Doval TL, Traore AK, Gallée H (2010) AMMA-model intercomparison project. Bull Am Meteorol Soc 91:95–104. doi:10.1175/2009BAMS2791.1

Hurtt GC, Frolking S, Fearon MG, Moore B III, Shevliakova E, Malyshev S, Pacala SW, Houghton RA (2006) The underpinnings of land-use history: three centuries of global gridded land-use transitions, wood harvest activity, and resulting secondary lands. Glob Change Biol 12:1208–1229. doi:10.1111/j.1365-2486.2006.01150.x

Hurtt GC, Chini LP, Frolking S, Betts R, Feddema J, Fischer G, Fisk JP, Hibbard K, Houghton RA, Janetos A, Jones C, Kindermann G, Kinoshita T, Klein Goldewijk K, Riahi K, Shevliakova E, Smith S, Stehfest E, Thomson A, Thornton P, van Vuuren DP, Wang Y (2011) Harmonization of land-use scenarios for the period 1500–2100: 600 Years of global gridded annual land-use transitions, wood harvest, and resulting secondary lands. Clim Change 109:117–161. doi:10.1007/s10584-011-0153-2

Iacono M, Delamere J, Mlawer E, Shephard M, Clough S, Collins W (2008) Radiative forcing by long-lived greenhouse gases: calculations with the AER radiative transfer models. J Geophys Res 113D:13103

IGBP (1992) Improved global data for land applications. In: Townshend JRG (ed) IGBP Global Change Report No 20. International Geosphere-Biosphere Programme, Stockholm

IPCC (2014) Climate change 2014: synthesis report. In: Pachauri RK, Meyer LA (eds) Contribution of working groups I, II and III to the fifth assessment report of the intergovernmental panel on climate change. IPCC, Geneva

Kanamitsu M, Ebisuzaki W, Woollen J, Yang SK, Hnilo JJ, Fiorino M, Potter GL (2002) NCEP–DOE AMIP-II reanalysis (R-2). Bull Am Meteorol Soc 83:1631–1643

Kang H-S, Xue Y, Collatz GJ (2007) Impact assessment of satellite-derived leaf area index datasets using a general circulation model. J Clim 20:993–1015. doi:10.1175/JCLI4054.1

Kim D-H, Sexton JO, Townshend JR (2014) Accelerated deforestation in the humid tropics from the 1990s to the 2000s. Geophys Res Lett 42:3495–3501. doi:10.1002/2014GL062777

Kim DH, Sexton JO, Noojipady P, Huang C, Anand A, Channan S, Feng M, Townshend JR (2015) Global, Landsat-based forest-cover change from 1990 to 2000. Remote Sens Environ 155:178–193

Koster RD, Dirmeyer PA, Guo Z, Bonan G, Chan E, Cox P, Gordon CT, Kanae S, Kowalczyk E, Lawrence D, Liu P, Lu CH, Malyshev S, McAvaney B, Mitchell K, Mocko D, Oki T, Oleson K, Pitman A, Sud YC, Taylor CM, Verseghy D, Vasic R, Xue Y, Yamada T (2004) Regions of strong coupling between soil moisture and precipitation. Science 305:1138–1140

Koster R, Suarez MJ, Ducharne A, Kumar P, Stieglitz M (2000) A catchment based approach to modeling land surface processes in a GCM—Part 1: model structure. J Geophys Res 105:809–822

Kuchler AW (1983) World map of natural vegetation. Goode's World Atlas, 16th edn. Rand McNally, pp 16–17

Laval K, Picon L (1986) Effect of a change of the surface albedo of the Sahel on climate. J Atmos Sci 43:2418–2429

Lawrence PJ, Chase TN (2007) Representing a new MODIS consistent land surface in the community land model (CLM 3.0). J Geophys Res 112:G01023. doi:10.1029/2006JG000168

Leblanc MJ, Favreau G, Massuel S, Tweed SO, Loireau M, Cappelaere B (2008) Land clearance and hydrological change in the Sahel: SW Niger. Glob Planet Change 61:135–150. doi:10.1016/j.gloplacha.2007.08.011

Li W, Xue Y, Poccard I (2007) Numerical investigation of the impact of vegetation indices on the variability of West African summer monsoon. J Meteorol Soc Jpn 85A:363–383

Mahmood R, Pielke RA Sr, Hubbard KG, Niyogi D, Dirmeyer PA, McAlpine C, Carleton AM, Hale R, Gameda S, Beltran-Przekurat A, Baker B, McNider R, Legates DR, Shepherd M, Du J, Blanken PD, Frauenfeld OW, Nair US, Fall S (2014) Land cover changes and their biogeophysical effects on climate. Int J Climatol 34:929–953. doi:10.1002/joc.3736

Mechoso CR, Yu JY, Arakawa A (2000) A coupled GCM pilgrimage: from climate catastrophe to ENSO simulations. General circulation model development: past, present and future. In: Proceedings of a symposium in honor of professor Akio Arakawa, D. A. Randall. Academic Press, USA, pp 539–575

Moorthi S, Suarez MJ (1992) Relaxed Arakawa-Schubert: a parameterization of moist convection for general circulation models. Mon Weather Rev 120:978–1002

Newell RE, Kidson JW (1984) African means wind changes between Sahelian wet and dry periods. Int J Climatol 4:27–33

Nicholson SE (2008) The intensity, location and structure of the tropical rain belt over West Africa as factors in interannual variability. Int J Climatol 28:1775–1785

Nicholson SE (2013) The West African Sahel: a review of recent studies on the rainfall regime and its variability. ISRN Meteorol. doi:10.1155/2013/453521

Nicholson SE, Grist JP (2001) A simple conceptual model for understanding rainfall variability in the West African Sahel on interannual and interdecadal time scales. Int J Climatol 21:1733–1757

Nicholson SE, Tucker CJ, Ba MB (1998) Desertification, drought, and surface vegetation: an example from the West African Sahel. Bull Am Meteorol Soc 79:1–15

Oleson KW, Niu GY, Yang ZL, Lawrence DM, Thornton PE, Lawrence PJ, Stöckli R, Dickinson RE, Bonan GB, Levis S, Dai A, Qian T (2008) Improvements to the community land model and their impact on the hydrological cycle. J Geophys Res 113:G01021. doi:10.1029/2007JG000563

Pielke RA Sr, Pitman A, Niyogi D, Mahmood R, McAlpine C, Hossain F, Goldewijk KK, Nair U, Betts R, Fall S, Reichstein M, Kabat P, de Noblet N (2011) Land use/land cover changes and climate: modeling analysis and observational evidence. WIREs Clim Change 2:828–850. doi:10.1002/wcc.144

Pitman AJ, de Noblet-Ducoudré N, Cruz FT, Davin EL, Bonan GB, Brovkin V, Claussen M, Delire C, Ganzeveld L, Gayler V et al (2009) Uncertainties in climate responses to past land cover

change: first results from the LUCID intercomparison study. Geophys Res Lett 36:L14814. doi:10.1029/2009GL039076

Ramankutty N, Evan A, Monfreda C, Foley JA (2008) Farming the planet: 1. Geographic distribution of global agricultural lands in the year 2000. Glob Biogeochem Cycles 22:GB1003. doi:10.1029/2007GB002952

Redelsperger J-L, Thorncroft CD, Diedhiou A, Lebel T, Parker DJ, Polcher J (2006) African monsoon multidisciplinary analysis: an international research project and field campaign. Bull Am Meteorol Soc 87:1739–1746

Roehrig R, Bouniol D, Guichard F, Hourdin F, Redelsperger J-L (2013) The present and future of the West African monsoon: a process-oriented assessment of CMIP5 simulations along the AMMA transect. J Clim 26:6471–6505. doi:10.1175/JCLI-D-12-00505.1

Saeed F, Hagemann S, Jacob D (2009) Impact of irrigation on the South Asian summer monsoon. Geophys Res Lett 36:L20711. doi:10.1029/2009GL040625

Santer BD, Wigley TML (1990) Regional validation of means, variances, and spatial patterns in general circulation model control runs. J Geophys Res 95:829–850

Song G (2013) Global and Sahel regional biophysical processes, vegetation dynamics, and climate interactions. PhD Dissertation. University of California, Los Angeles, p 183

Sud YC, Fennessy M (1982) A study of the influence of surface albedo on July circulation in semi-arid regions using the GLAS GCM. J Climatol 2:105–125

Taylor CM, Parker DJ, Kalthoff N, Gaertner MA, Philippon N, Bastin S, Harris PP, Boone A, Guichard F, Flamant C, Grandpeix J-Y, Cerlini P, Baldi M, Descroix L, Douville H, Polcher J, Agusti-Panareda A (2011) New perspectives on land-atmosphere feedbacks from the African monsoon multidisciplinary analysis (AMMA). Atmos Sci Lett 12:38–44. doi:10.1002/asl.336

Taylor CM, de Jeu RichardAM, Guichard F, Harris PP, Dorigo WA (2012a) Afternoon rain more likely over drier soils. Nature 489:423–426. doi:10.1038/nature11377

Taylor KE, Stouffer RJ, Meehl GA (2012b) An overview of CMIP5 and the experiment design. Bull Am Meteorol Soc 93:485–498. doi:10.1175/BAMS-D-11-00094.1

Tuinenberg OA, Hutjes RWA, Kabat P (2012) The fate of evaporated water from the Ganges basin. J Geophys Res. doi:10.1029/2011JD016221

Wang GL, Eltahir EAB (2000) The role of ecosystem dynamics in enhancing the low-frequency variability of the Sahel rainfall. Water Resour Res 36(4):1013–1021

Wang G, Yu M, Xue Y (2015) Modeling the potential contribution of land use changes to the 20th century Sahel drought using a regional climate model: impact of lateral boundary conditions. Clim Dyn 34:929–953. doi:10.1007/s00382-015-2812-x

Wei J, Dirmeyer PA, Wisser D, Bosilovich MJ, Mocko DM (2013) Where does the irrgation water go? An estimate of the contribution of iirgation to precipitation using MERRA. J Hydrometeorol 14:275–289. doi:10.1175/JHM-D-12-079.1

Xue Y (1997) Biosphere feedback on regional climate in tropical North Africa. Q J R Meteorol Soc 123:1483–1515

Xue Y, Dirmeyer PA (2015) Land-atmosphere interactions in monsoon regimes and future prospects for enhancing prediction. CLIVAR Exchanges 19(66):28–33

Xue Y, Liou KN, Kasahara A (1990) Investigation of the biogeophysical feedback on the African climate using a two-dimensional model. J Clim 3:337–352

Xue Y, Sellers PJ, Kinter JL, Shukla J (1991) A simplified biosphere model for global climate studies. J Clim 4:345–364

Xue Y, Juang HM, Li W, Prince S, DeFries R, Jiao Y, Vasic R (2004) Role of land surface processes in monsoon development: East Asia and West Africa. J Geophys Res 109:D03105. doi:10.1029/2003JD003556

Xue Y, De Sales F, Lau KMW, Boone A, Feng J, Dirmeyer P, Guo Z, Kim KM, Kitoh A, Kumar V, Poccard-Leclercq I, Mahowald N, Moufouma-Okia W, Pegion P, Rowell D, Schubert SD, Sealy A, Thiaw WM, Vintzileos A, Williams S, Wu MLC (2010a) Intercomparison and analyses of the climatology of the West African monsoon in the West African Monsoon Modeling and Evaluation project (WAMME) First Model Intercomparison Experiment. Clim Dyn 35:3–27. doi:10.1007/s00382-010-0778-2

Xue Y, De Sales F, Vasic R, Mechoso CR, Prince SD, Arakawa A (2010b) Global and temporal characteristics of seasonal climate/vegetation biophysical processes (VBP) interactions. J Clim 23:1411–1433

Xue Y, Boone A, Taylor CM (2012) Review and prospective of recent development in West African atmosphere/land interaction studies. Int J Geophys. doi:10.1155/2012/748921

Xue Y, De Sales F, Lau WK-M, Boone A, Kim K-M, Mechoso CR, Wang G, Kucharski F, Schiro K, Hosaka M, Li S, Druyan LM, Seidou Sanda I, Thiaw W, Zeng N, Comer RE, Lim Y-K, Mahanama S, Song G, Gu Y, Hagos SM, Chin M, Schubert S, Dirmeyer P, Leung LR, Kalnay E, Kitoh A, Lu C-H, Mahowald NM, Zhang Z (2016) West African monsoon decadal variability and surface-related forcings: second West African Monsoon Modeling and Evaluation project experiment (WAMME II). Clim Dyn. doi:10.1007/s00382-016-3224-2

Zhang GJ, McFarlane NA (1995) Sensitivity of climate simulations to the parameterization of cumulus convection in the Canadian climate centre general circulation model. Atmos Ocean 33:407–446

Zhang Z, Xue Y, MacDonald G, Cox PM, Collatz GJ (2015) Investigation of North American vegetation variability under recent climate—a study using the SSiB4/TRIFFID biophysical/dynamic vegetation model. J Geophy Res 120:1300–1321. doi:10.1002/2014JD021963

Zheng XY, Eltahir EAB (1997) The response to deforestation and desertification in a model of West African monsoons. Geophys Res Lett 24:155–158